Simplified load-deflection behavior of cracked prestressed concrete beams based on a rigorous formulation

Kimberly Waggle Kramer, Hayder A. Rasheed, and Steven R. Peterson

- This paper presents equations for predicting midspan deflections and moment-curvature behavior for prestressed concrete beams from an uncracked state through cracking, yielding, and ultimate loading.
- Trilinear moment curvature was used to develop closed-form analytical deflection expressions for simply supported prestressed concrete girders subjected to different loading conditions.
- The predicted deflections and structural response from the proposed method were compared with experimental data from the literature and found to have good correlation with published experimental results.

The flexural behavior of prestressed concrete beams is complex, and a simplified method for calculating deflections due to short-term loads is desirable. Various procedures have been proposed to determine the immediate deflection of cracked prestressed concrete components.[1,2] The procedures from the eighth edition of the *PCI Design Handbook: Precast and Prestressed Concrete*[3] for instantaneous deflection of prestressed concrete components are based on the bilinear moment-deflection relationship or the effective moment of inertia method. The American Concrete Institute's (ACI's) *Building Code Requirements for Structural Concrete (ACI 318-19) and Commentary (ACI 318R-19)*[4] uses the second approach (effective moment of inertia method); however, the ACI 318-19 commentary references the first approach of *PCI Design Handbook*[3] (bilinear moment-deflection relationship) as a viable alternative. Both procedures accurately predict instantaneous deflections for prestressed concrete components in the working load range; however, at higher loads, these prediction methods become inaccurate.[5]

Kramer and Rasheed[5] investigated the analytical load deflection of prestressed concrete girders strengthened with externally bonded carbon-fiber-reinforced polymer sheets. They compared analytical and numerical moment-curvature responses for prestressed concrete T beams with bonded strands, and they concluded that the analytically assumed trilinear moment-curvature function—which represents the foundation for establishing the short-term deflection expressions—accurately predicts moment-curvature and short-term

load-deflection responses of prestressed concrete flexural components with bonded and straight strands strengthened with externally bonded fiber-reinforced polymers sheets.

This paper evaluates a proposed method in which a trilinear moment-curvature response is used to obtain closed-form analytical deflection expressions for simply supported prestressed concrete girders subjected to different loading conditions up to failure. This proposed trilinear method predicts instantaneous deflections at loads that exceed the yielding of prestressing strands more accurately than current state of the art methods.

Analytical investigation

The moment-curvature response of prestressed concrete components can be approximately modeled by a trilinear relationship. This relationship can be fully determined by applying standard linear and nonlinear sectional analysis equations at cracking, yielding, and ultimate levels. The general solution can be obtained by adding the deflection contribution of the three regions, as shown in Eq. (1).

$$\Delta_{midspan} = \delta_1 + \delta_2 + \delta_3 = \int_0^{L_g} x\phi_{un}(x)\,dx + \int_{L_g}^{L_y} x\phi_{cr-y}(x)\,dx + \int_{L_y}^{\frac{L}{2}} x\phi_{y-n}(x)\,dx \quad (1)$$

where

$\Delta_{midspan}$ = midspan deflection

δ_1 = deflection for the uncracked region

δ_2 = deflection for the postcracked region

δ_3 = deflection for the postyielding region

L_g = length from the support to the cracking moment location (uncracked region)

x = location along the beam measured from the support

$\phi_{un}(x)$ = curvature expression for the uncracked region

L_y = length from the support to the yield moment location

$\phi_{cr-y}(x)$ = curvature expression for the postcracked region

L = span length

$\phi_{y-n}(x)$ = curvature expression for the postyielding region

Assumptions

The analysis presented herein is based on several assumptions about material behavior, sectional behavior, and member behavior that are used to accurately simplify deflection calculations. These assumptions are as follows:

- When the cracking load limit is calculated, the stress-strain relationship for concrete in compression is considered linear, with a modulus of elasticity of the concrete E_c.
- Hognestad's parabolic equation[6] is used when concrete in compression is analyzed at yielding and ultimate levels.
- The stress-strain relationship for the prestressing reinforcement is adopted from the expressions in the *PCI Design Handbook*[3] for 270 or 250 ksi (1860 or 1720 MPa), low-relaxation, seven-wire strands.
- The stress-strain relationship for mild steel compression reinforcement is assumed to be elastic–perfectly plastic with yielding stress given or assumed for the mild steel reinforcement.
- The strain is distributed linearly across the cross-section depth following Bernoulli's hypothesis of a plane section remaining plane after bending.
- The crushing failure of concrete in compression occurs at a strain of 0.003.[4]
- Prestressing strand yields at a strain 0.01, and prestressing strand ultimate strain is assumed to occur at a strain of 0.05. These values for yielding and rupture are taken from Design Aid 15.2.3 in the eighth edition of the *PCI Design Handbook*.[3]
- The concrete is considered cracked when the extreme bottom stress is greater than the concrete rupture strength

  fr: $f_r = 7.5\sqrt{f'_c}$ psi or $f_r = 0.62\sqrt{f'_c}$ N/mm^2,[4] where f'_c is the compressive
- strength of concrete. By using a linear moment-curvature relationship between the cracking and yielding points, some tension stiffening effects after rupture have been considered.
- The smeared cracked analysis procedure is used to determine average curvatures of the cracked members.
- The prestressing reinforcement is assumed to be straight and fully bonded to the concrete.
- Mild tension reinforcing steel is ignored in this analysis.

Moment-curvature relationship

The moment-curvature response is idealized to be trilinear with precracked, postcracked, and postyielding stages. The first stage extends to the onset of flexural cracking. The second stage is from cracking to the first yielding of the prestressing steel. The third stage continues until the limit of the concrete's useful strain of 0.003 (concrete crushing) or the prestressing strand's useful strain of 0.05 (strand rupture). The

moment-curvature relationship is fully defined when ($M_a = 0$, ϕ_{in}), (M_{cr}, ϕ_{cr}), (M_y, ϕ_y), and (M_n, ϕ_n) are determined (**Fig. 1**), where M_a is moment at the load application point, ϕ_{in} is initial curvature, M_{cr} is cracking moment, ϕ_{cr} is curvature at the cracking moment location, M_y is moment at yield, ϕ_y is yield point curvature, M_n is nominal ultimate moment, and ϕ_n is curvature at the nominal ultimate moment location

Initial point The initial moment curvature point is a theoretical point in which the total external moment is zero. In essence, the member is considered to be weightless and the only moment is provided internally by the prestressing force P_e multiplied by its eccentricity e to the center of gravity of the transformed section. The stresses in the extreme bottom f_{bot} and top fibers f_{top} for the section are determined through internal stress analysis (Eq. [2] and [3]), with compressive stresses considered negative and tensile stresses considered positive and the eccentricity e being positive when the initial prestressing force is below the center of gravity.

$$f_{bot} = \frac{-P_e}{A_{gt}} - \frac{P_e e y_{bot}}{I_{gt}} \quad (2)$$

where

A_{gt} = gross area of the transformed section

y_{bot} = distance from the bottom of the section to the neutral axis

I_{gt} = gross moment of inertia of the transformed section

$$f_{top} = \frac{-P_e}{A_{gt}} + \frac{P_e e y_{top}}{I_{gt}} \quad (3)$$

where

y_{top} = distance from the top of the section to the neutral axis

When the section is uncracked, strains at the bottom of the section ε_{bot} and the top of the section ε_{top} are determined by dividing the stresses in Eq. (2) and (3) by the modulus of elasticity of the concrete E_c. The initial point is defined by the initial curvature ϕ_{in} and externally applied moment M_a given by Eq. (4) and (5), respectively. The curvature equation (Eq. [4]) is determined by subtracting the top strain from the bottom strain and dividing the difference by the height of the component h.

$$\phi_{in} = \frac{-P_e e}{I_{gt} E_c} \quad (4)$$

$$M_a = 0 \quad (5)$$

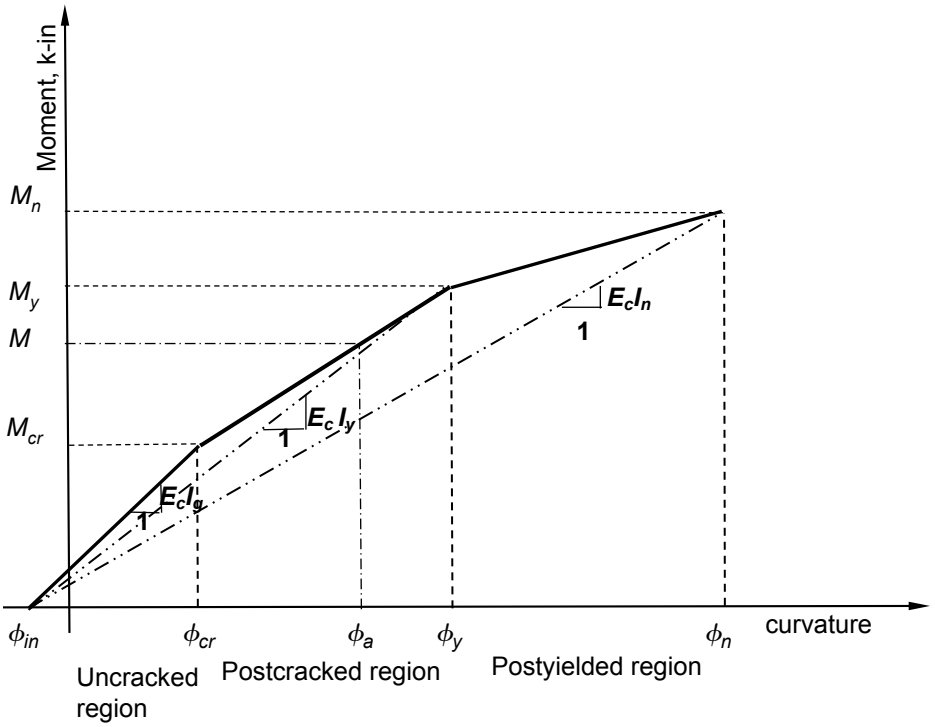

Figure 1. Trilinear moment-curvature behavior of prestressed concrete beams.
Note: E_c = modulus of elasticity of concrete; I_g = gross moment of inertia; I_n = moment of inertia at the nominal ultimate moment; I_y = moment of inertia at yield; M = moment; M_{cr} = cracking moment; M_n = nominal ultimate moment; M_y = moment at yield; ϕ_a = curvature at the point of load application; ϕ_{cr} = curvature at the cracking moment location; ϕ_{in} = initial curvature; ϕ_n = curvature at the nominal ultimate moment location; ϕ_y = curvature at yield.

Cracking point The cracking moment–curvature point is the end of the linear-elastic response for the component. For all sections, the cracking point occurs when the bottom extreme fiber just reaches the cracking stress (concrete rupture strength). The cracking stress f_r is set equal to extreme bottom fiber stress because the component under consideration is loaded from the top. The cracking stress is determined in accordance with *Building Code Requirements for Structural Concrete (ACI 318-19) and Commentary (ACI 318R-19)*,[4] as shown in Eq. (6).

$$f_r = 7.5\sqrt{f'_c} \tag{6}$$

where

f'_c is in psi

For the analysis, the self-weight of the member is considered an external load and is combined with other external loading to determine the external moment. The stresses are distributed linearly across the cross section. The analysis procedure is similar to the analysis for the initial point, with the bottom and top strains defined by Eq. (7) and (8).

$$\varepsilon_{bot} = \frac{-P_e}{A_{gt}E_c} - \frac{P_e e y_{bot}}{I_{gt}E_c} + \frac{M_{cr} y_{bot}}{I_{gt}E_c} \tag{7}$$

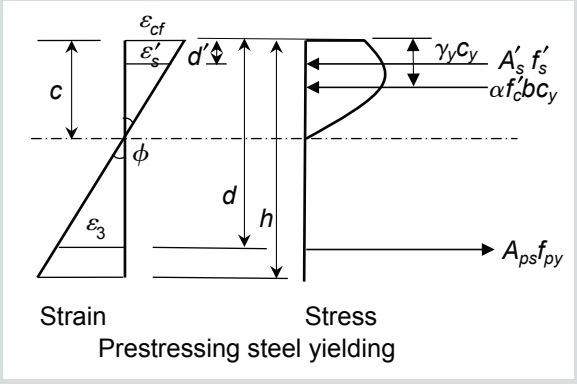

Figure 2. Section strain-compatibility relationships at yielding of prestressing steel.
Note: A_{ps} = area of prestressing steel; A'_s = area of compression reinforcement; b = section width; c_y = depth of the section neutral axis at first yielding; d = depth from the top of the section to the prestressing steel; d' = depth from the top of the section to the compression reinforcement; f'_c = design compressive strength of concrete; f_{py} = yield stress of the prestressing steel; f'_s = stress in the compression reinforcement; h = height of the section; α = factor for the height of the equivalent rectangular stress block; γ_y = neutral axis multiplier corresponding to c_y; ε_{cf} = extreme compressive fiber strain; ε'_s = strain in the compression reinforcing steel; ε_1 = strain due to the initial tensioning stress in the prestressing steel after losses; ε_2 = strain due to the decompression of the section at the level of the prestressing strands; ε_3 = remaining strain in the prestressing strand required for strain compatibility (after accounting for ε_1 and ε_2); ϕ_y = yield point curvature.

$$\varepsilon_{top} = \frac{-P_e}{A_{gt}E_c} + \frac{P_e e y_{top}}{I_{gt}E_c} - \frac{M_{cr} y_{top}}{I_{gt}E_c} \tag{8}$$

The cracking point is defined by the cracking curvature ϕ_{cr} (Eq. [9]) and the externally applied moment causing cracking M_{cr} (Eq. [10]).

$$\phi_{cr} = \frac{-\left(P_e e - M_{cr}\right)}{I_{gt}E_c} \tag{9}$$

$$M_{cr} = \frac{\left(f_r A_{gt} + P_e\right) r^2}{y_{bot}} + P_e e \tag{10}$$

where

r^2 = the square of the radius of gyration

Yielding point The yielding point occurs as the prestressing steel reaches the yielding strain of 1% elongation specified in the *PCI Design Handbook*.[3] Because the strain in the prestressing steel ε_{ps} is significantly greater than the cracking strain of the concrete, the section is defined as cracked at strand yielding. Strain-compatibility analysis is used at this stage. **Figure 2** depicts the section strain-compatibility relationships at prestressing steel yielding. As shown in Eq. (11), (12), and (13), this strain has three components: the strain ε_1 due to the initial tensioning stress in the prestressing steel f_{se} after losses; strain ε_2 due to the decompression of the section at the level of the prestressing strands; and strain ε_3, which is the remaining strain due to strain compatibility at strand yielding with the yield strain of the prestressing steel ε_{psy} equal to 0.01.

$$\varepsilon_1 = \frac{f_{se}}{E_{ps}} \tag{11}$$

where

E_{ps} = modulus of elasticity of the prestressing strands

$$\varepsilon_2 = \frac{1}{E_{ps}}\left[\frac{P_e}{A_{gt}} + \frac{P_e e^2}{I_{gt}}\right] \tag{12}$$

$$\varepsilon_3 = 0.01 - \varepsilon_1 - \varepsilon_2 \tag{13}$$

The extreme compression fiber strain ε_{cf} is determined using strain compatibility (Eq. [14]).

$$\varepsilon_{cf} = \frac{\varepsilon_3 c_y}{\left(d - c_y\right)} \tag{14}$$

where

c_y = depth of the section neutral axis at first yielding

d = depth from the top of the section to the prestressing steel

The depth of the section neutral axis at first yielding c_y is unknown and is solved from the force equilibrium of the cross section. After establishing the steel-concrete strain relation-

ship, Hognestad's parabolic stress-strain equation6 is invoked to furnish concrete compressive stresses at any concrete fiber, as shown in Eq. (15):

$$f_c = f'_c\left[2\frac{\varepsilon_c}{\varepsilon'_c} - \left(\frac{\varepsilon_c}{\varepsilon'_c}\right)^2\right] \tag{15}$$

where

f_c = concrete compressive stress

ε_c = concrete strain

ε'_c = strain at maximum compressive stress

The stress distribution is converted into an equivalent rectangular stress block by Eq. (16).[7]

$$f_c = \alpha f'_c = f'_c\left[\frac{\varepsilon_{cf}}{\varepsilon'_c} - \frac{\left(\varepsilon_{cf}\right)^2}{3\left(\varepsilon'_c\right)^2}\right] \tag{16}$$

where

α = factor for the height of the equivalent rectangular block

Because the centroid of the actual compressive stress is based on a parabolic shape, the location of the compression force is placed a distance of γc_y from the extreme compressive fiber. The neutral axis multiplier γ is given by Eq. (17).[8]

$$\gamma = \frac{\frac{1}{3} - \frac{\varepsilon_{cf}}{12\varepsilon'_c}}{1 - 3\frac{\varepsilon_{cf}}{\varepsilon'_c}} \tag{17}$$

In additionlly, the neutral axis multiplier is dependent on the strain at maximum compressive stress and the extreme compressive fiber strain ε_{cf}, which was previously defined in Eq. (14).

After the steel and concrete stress-strain relationships are known, the distance from the extreme fiber in compression to the neutral axis c_y is found by force equilibrium. The equations for determining c_y are dependent on the cross-sectional shape and the inclusion of mild compression steel. Therefore, rectangular, T section, and I-section layouts, both with and without mild compression reinforcement, are discussed in the following sections. The derivations of the moment-curvature equations for the T section and I-section are the same, as the lower flange of the I-section is neglected due to cracking.

When considering the yielding point moment-curvature equations, the simplest derivation pertains to the rectangular cross section without mild compression steel. This derivation is the simplest because the width remains constant, enabling the representation of the concrete compressive force by a single force, irrespective of the c_y location, and the compression force is provided solely by the concrete. Consequently, equilibrium in the cross section demands the balancing of two forces: the concrete compressive force C and the tension force T from prestressing steel, as defined by Eq. (18) and (19), respectively.

$$C = \alpha f'_c c_y b = \frac{\varepsilon_3\left(c_y\right)^2 f'_c b}{\varepsilon'_c\left(d - c_y\right)} - \frac{\left(\varepsilon_3\right)^2\left(c_y\right)^3 f'_c b}{3\left(\varepsilon'_c\right)^2\left(d - c_y\right)} \tag{18}$$

where

b = section width

$$T = A_{ps} f_{ps} = A_{ps}\left(f_{pu} - \frac{0.04}{0.01 - x_1}\right) \tag{19}$$

where

A_{ps} = area of prestressing steel

f_{ps} = stress in the prestressing steel

f_{pu} = ultimate stress of the prestressing steel

x_1 = constant based on the yield strength of the prestressing strand (x_1 = 0.0064 for 250 ksi prestressing strand and x_1 = 0.0070 for 270 ksi prestressing strand)

After the forces are defined in terms of c_y, c_y is calculated by Eq. (20).

$$\begin{aligned}&\left(\left(3\varepsilon_3\varepsilon'_c + \left(\varepsilon_3\right)^2\right) f'_c b\right)\left(c_y\right)^3 + \left(3A_{ps} f_{ps}\left(\varepsilon'_c\right)^2 - 3\varepsilon_3 f'_c b\varepsilon'_c d\right)\left(c_y\right)^2 \\ &-\left(6A_{ps} f_{ps}\left(\varepsilon'_c\right)^2 d\right)c_y + 3A_{ps} f_{ps}\left(\varepsilon'_c\right)^2 d^2 = 0\end{aligned} \tag{20}$$

After the location of the neutral axis is defined, the strain at the extreme compression fiber is determined and the yield point curvature ϕ_y is found by Eq. (21).

$$\phi_y = \frac{\varepsilon_{cf}}{c_y} = \frac{\varepsilon_3}{\left(d - c_y\right)} \tag{21}$$

The corresponding moment for the yield point is found by summing the prestressing moment about the centroid of the compressive force (Eq. [22]).

$$M_y = T(d - \gamma_{cy}) = A_{ps} f_{ps}(d - \gamma c_y) \tag{22}$$

When mild reinforcing steel is in the compression region, Eq. (18) through (22) are amended with a force contribution from the mild compression steel. The strain in the mild compression steel ε'_s is given by Eq. (23). The force in the compression steel C_s depends on whether the compression steel has yielded (Eq. [24]) or not (Eq. [25]).

$$\frac{\varepsilon'_s}{\left(c_y - d'\right)} = \frac{\varepsilon_3}{\left(d - c_y\right)} \Rightarrow \varepsilon'_s = \frac{\varepsilon_3\left(c_y - d'\right)}{\left(d - c_y\right)} \tag{23}$$

where

d' = depth from the top of the section to the compression reinforcement

If the compression steel has yielded, then

$$C_s = A_s' f_y \tag{24}$$

where

A_s' = area of compression reinforcement

f_y = yield stress of the mild reinforcement

If the compression steel has not yielded, then

$$C_s = A_s' E_s \varepsilon_3 \frac{\left(c_y - d'\right)}{\left(d - c_y\right)} \tag{25}$$

where

E_s = modulus of elasticity of the mild reinforcement

The yielding moment is defined in Eq. (26) if the compression steel has not yielded or Eq. (27) if the compression steel has yielded.

$$M_y = A_{ps} f_{ps}\left(d - \gamma c_y\right) + A_s' E_s \frac{\varepsilon_3\left(c_y - d'\right)}{\left(d - c_y\right)}\left(\gamma c_y - d'\right) \tag{26}$$

$$M_y = A_{ps} f_{ps}\left(d - \gamma c_y\right) + A_s' f_y\left(\gamma c_y - d'\right) \tag{27}$$

When deriving the moment-curvature equations applicable to prestressed concrete T and I-sections with or without mild compression steel, the previous equations presented for the determination of c_y remain valid. When the section cracks, the tensile capacity of the concrete is disregarded. At the yielding point, the lower flange of the I-section is in the tension zone of the cracked cross section and can be disregarded. The only tension force is provided by the prestressing steel as described in Eq. (19). Given the nonuniform width of T and I-sections, the neutral axis may be located in the flange or the web. If the neutral axis is in the web, the variation in the cross-sectional width is considered by separating the compression force into two forces C_1 and C_2 for deriving the moment-curvature equations. The first compressive force C_1 is a positive compressive force derived by using the depth of the neutral axis, cy, multiplied by the entire flange width. The second compressive force C_2 is a negative compressive force to eliminate the overestimation of the first compressive force caused by the two voids on both sides of the projected web with a width of $(b_f - b_w)$ and a depth of $(c_y - t_f)$ (**Fig. 3**).

The strains for the prestressing steel in the I-section or T section are found by Eq. (11) through (13), and the extreme compressive fiber strain is found by Eq. (14); however, it is necessary to determine the strain at the compressive flange–web junction because that strain is used in determining the second compressive force C_2.

From the linear strain distribution in Fig. 3 and strain compatibility, the strain at the compressive flange-web junction ε_{cw} is given by Eq. (28).

$$\varepsilon_{cw} = \frac{\varepsilon_3\left(c_y - t_f\right)}{\left(d - c_y\right)} \tag{28}$$

where

t_f = flange thickness

After this strain is determined, the stress-strain relationships for the negative compressive force C_2 can be obtained. By integrating Hognestad's equation from zero strain to the strain at the compressive flange–web junction, then dividing by the strain at the flange-web junction, α_2 is determined by Eq. (29).

$$f_{cw} = \alpha_2 f_c' = f_c'\left[\frac{\varepsilon_{cw}}{\varepsilon_c'} - \frac{(\varepsilon_{cw})^2}{3(\varepsilon_c')^2}\right] \Rightarrow \alpha_2 = \left[\frac{\varepsilon_{cw}}{\varepsilon_c'} - \frac{(\varepsilon_{cw})^2}{3(\varepsilon_c')^2}\right] \tag{29}$$

where

α_2 = proportional factor for the height of the equivalent rectangular stress block corresponding to C_2

For clarification purposes, the proportional term for C_2 is labeled α_2. In addition, the negative compressive force is placed at a distance $\gamma_2(c_y - t_f)$ from the compressive flange–web junction. The neutral axis multiplier γ_2 is given by Eq. (30).[8]

$$\gamma_2 = \frac{\frac{1}{3} - \frac{\varepsilon_{cw}}{12\varepsilon_c'}}{1 - 3\frac{\varepsilon_{cw}}{\varepsilon_c'}} \tag{30}$$

The magnitude and placement of the compressive force C_1 (Eq. [31]) are the same as for the concrete compressive force C for a rectangular section. Eq. (16) and (17) are used to determine the proportional term α_1 and neutral axis multiplier γ_1 for C_1. On the other hand, the parameter α_2 and γ_2 uses the same Eq. (16) and (17) while replacing the extreme fiber strain ε_{cf} with a strain at the flange-web junction ε_{cfw}. See Eq. (32).

$$C_1 = \alpha_1 f_c' c_y b_f \tag{31}$$

where

b_f = flange width

$$C_2 = \alpha_2 f_c'\left(c_y - t_f\right)\left(b_f - b_w\right) \tag{32}$$

where

b_w = web width

$\varepsilon_{cw} - f_w$ = strain at the flange-web junction, equal to $\varepsilon_{cf} / c_y \times (c_y - t_f)$

Substituting Eq. (19), (31), and (32) into the force equilibrium equation, c_y can be directly determined by Eq. (33).

$$(c_y)^3\left[\left(3\varepsilon_c' + \varepsilon_3\right) f_c' b_w\right] + (c_y)^2$$
$$\left[\left(-3\varepsilon_c' d f_c' b_w + \left(6\varepsilon_c' t_f + 3\varepsilon_3 t_f\right)\right) f_c'\left(b_f - b_w\right) - \frac{3A_{ps} f_{ps} (\varepsilon_c')^2}{\varepsilon_3}\right]$$
$$+ c_y\left[\left(-3\varepsilon_c'\left(2dt_f + (t_f)^2\right) - 3\varepsilon_3 (t_f)^2\right) f_c'\left(b_f - b_w\right) - \frac{6A_{ps} f_{ps} (\varepsilon_c')^2 d}{\varepsilon_3}\right]$$
$$+\left[\left(3\varepsilon_c' (t_f)^2 d + \varepsilon_3 (t_f)^2\right) f_c'\left(b_f - b_w\right) + \frac{3A_{ps} f_{ps} (\varepsilon_c')^2 d^2}{\varepsilon_3}\right] = 0 \quad (33)$$

The curvature is determined from Eq. (21). The corresponding moment for the yielding point is found by summing the moments about the centroid of the tension force.

The final yield moment equation for an I-section or T section without mild compression steel is given by Eq. (34).

$$M_y = \alpha_1 f_c' c_y b_f \left(d - \gamma_1 c_y\right) - \alpha_2 f_c'\left(c_y - t_f\right)\left(b_f - b_w\right)\left(c_y - t_f\right)\left(d - t_f - \gamma_2 c_y\right) \quad (34)$$

As with the T section having no mild compression steel, the derivation of compressive stresses depends on whether the neutral axis is in the flange or in the web. When the neutral axis goes into the web, the compression force is composed of the forces C_1, C_2, and C_s. **Figure 4** shows the linear strain distribution used to determine the strains. The stress-strain relationships and the compression force equations for the mild compression steel have been previously presented in Eq. (23), (24), and (25).

After the neutral axis is located, the curvature is found using Eq. (21), and the corresponding moment is found by summing the moments about the centroid of the tension force. If the mild compression steel has not yielded, the final moment is determined by Eq. (35).

$$M_y = \alpha_1 f_c' c_y b_f \left(d - \gamma_1 c_y\right) - \alpha_2 f_c'\left(c_y - t_f\right)\left(b_f - b_w\right)\left(d - t_f - \gamma_2 c_y\right) + A_s' E_s \frac{\varepsilon_3 \left(c_y - d'\right)\left(d - d'\right)}{\left(d - c_y\right)} \quad (35)$$

If the mild compression steel has yielded, the final moment is determined by Eq. (36).

$$M_y = \alpha_1 f_c' c_y b_f \left(d - \gamma_1 c_y\right) - \alpha_2 f_c'\left(c_y - t_f\right)\left(b_f - b_w\right)\left(c_y - t_f\right)\left(d - t_f - \gamma_2 c_y\right) + A_c' f_y \left(d - d'\right) \quad (36)$$

Ultimate point The ultimate moment-curvature point is determined based on the mode of failure (strand rupture of the prestressing steel or crushing of the concrete). The crushing of the concrete is taken when the ultimate concrete useful strain equals 0.003 in accordance with ACI 318-19.[4] Accordingly, the

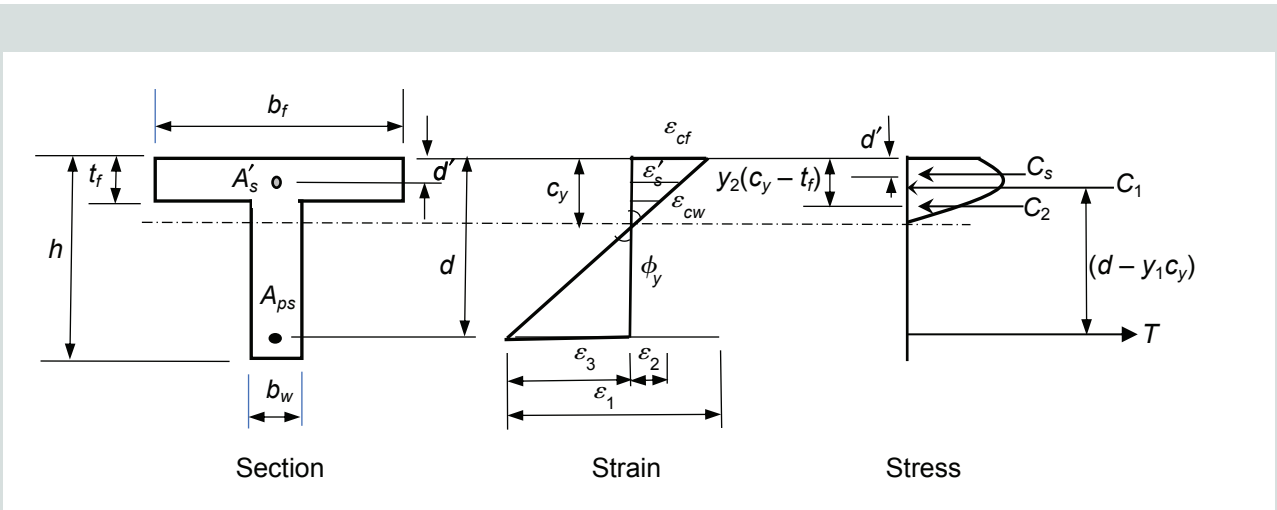

Figure 3. Stress and strain diagram for a T section with mild compression steel at first yielding.
Note: A_{ps} = area of prestressing steel; A_s' = area of compression reinforcement; b_f = flange width; b_w = web width; c_y = depth of the section neutral axis at first yielding; C_s = compressive force in the compression reinforcement; C_1 = first compressive force; C_2 = second compressive force; d = depth from the top of the section to the prestressing steel; d' = depth from the top of the section to the compression reinforcement; h = height of the section; t_f = flange thickness; T = tensile force; γ_1 = neutral axis multiplier corresponding to C_1; γ_2 = neutral axis multiplier corresponding to C_2; ε_{cf} = extreme compressive fiber strain; ε_{cw} = the strain at the compressive flange-web junction; ε_s' = strain in the compression reinforcement; ε_1 = strain due to the initial tensioning stress in the prestressing steel after losses; ε_2 = strain due to the decompression of the section at the level of the prestressing strands; ε_3 = remaining strain in the prestressing strand required for strain compatibility; ϕ_y = yield point curvature.

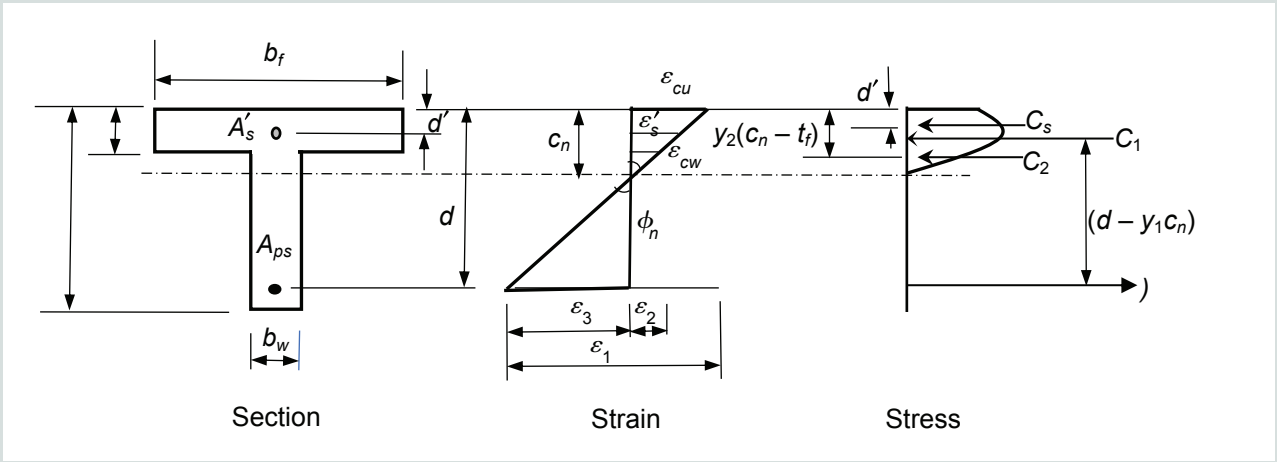

Figure 4. Stress and strain distributions for a T section with mild compression steel at concrete crushing failure mode. Note: A_{ps} = area of prestressing steel; A_s' = area of compression reinforcement; b_f = flange width; b_w = web width; c_n = depth of the section neutral axis at ultimate strength; C_s = compressive force in the compression reinforcement; C_1 = first compressive force; C_2 = second compressive force; d = depth from the top of the section to the prestressing steel; d' = depth from the top of the section to the compression reinforcement; h = height of the section; t_f = flange thickness; T = tensile force; γ_1 = neutral axis multiplier corresponding to C_1; γ_2 = neutral axis multiplier corresponding to C_2; ε_{cf} = extreme compressive fiber strain; ε_{cw} = the strain at the compressive flange-web junction; ε_{ps} = strain in the prestressing strand; ε_s' = strain in the compression reinforcement; ε_2 = strain due to the decompression of the section at the level of the prestressing strands; ε_3 = remaining strain in the prestressing strand required for strain; ϕ_n = curvature at the nominal ultimate moment.

concrete compression block depth is obtained from the force equilibrium and strain compatibility equations. These equations vary depending on whether the compression block is rectangular or T-shaped and whether the compression steel has yielded.

Based on the *PCI Design Handbook*,[3] the prestressing steel is assumed to rupture at a strain of 0.05. The rest of the conditions remain the same as with the yielding point. At the ultimate point, the neutral axis c_n for a rectangular stress block is determined by Eq. (37) through (39); these equations are also valid for a T section with the compression block within the flange when the section width b is replaced with b_f.

Eq. (37) is used to determine the neutral axis for a parabolic stress distribution in a rectangular section with no compression steel.

$$\left(\left(3\varepsilon_3\varepsilon_c' + \left(\varepsilon_3\right)^2\right)f_c'b\right)\left(c_n\right)^3 + \left(3A_{ps}f_{ps}\left(\varepsilon_c'\right)^2 - 3\varepsilon_3 f_c'b\varepsilon_c'd\right)$$
$$\left(c_n\right)^2 - \left(6A_{ps}f_{ps}\left(\varepsilon_c'\right)^2 d\right)c_n + 3A_{ps}f_{ps}\left(\varepsilon_c'\right)^2 d^2 = 0 \quad (37)$$

The neutral axis for a parabolic stress distribution in a rectangular section and with compression steel that has not yielded is determined using Eq. (38).

$$\left[\left(\varepsilon_3\varepsilon_c' + \left(\varepsilon_3\right)^2\right)f_c'b\right]\left(c_n\right)^3$$
$$+\left(A_{ps}f_{ps}\left(\varepsilon_c'\right)^2 - \varepsilon_3 f_c'b\varepsilon_c'd + A_s'E_s\varepsilon_3\left(\varepsilon_c'\right)^2\right)\left(c_n\right)^2$$
$$-\left[2A_{ps}f_{ps}\left(\varepsilon_c'\right)^2 d + A_c'E_s\varepsilon_3\left(\varepsilon_c'\right)^2\left(d + d'\right)\right]c_n$$
$$+\left(A_{ps}f_{ps}\left(\varepsilon_c'\right)^2 d^2 + A_c'E_s\varepsilon_3\left(\varepsilon_c'\right)^2 d'd\right) = 0 \quad (38)$$

Equation (39) determines the neutral axis for a parabolic stress distribution in a rectangular section with compression steel that has yielded.

$$\left[\left(\varepsilon_3\varepsilon_c' + \left(\varepsilon_3\right)^2\right)f_c'b\right]\left(c_n\right)^3$$
$$+\left(A_{ps}f_{ps}\left(\varepsilon_c'\right)^2 - \varepsilon_3 f_c'b\varepsilon_c'd + A_s'f_y\left(\varepsilon_c'\right)^2\right)\left(c_n\right)^2 \quad (39)$$

After the location of the neutral axis is defined, the strain at the extreme compression fiber is determined and the ultimate point curvature ϕ_{nr} is found by Eq. (40).

$$\phi_{nr} = \frac{\varepsilon_{cf}}{c_n} = \frac{\varepsilon_3}{\left(d - c_n\right)} = \frac{0.05 - \varepsilon_1 - \varepsilon_2}{\left(d - c_n\right)} \quad (40)$$

For the parabolic stress distribution in a rectangular section, Eq. (41), (42), and (43) are used to calculate the moment for no compression steel, compression steel not yielded, and compression steel yielded, respectively.

$$M_n = T\left(d - \gamma c_n\right) = A_{ps}f_{ps}\left(d - \gamma c_n\right) \quad (41)$$

$$M_n = A_{ps}f_{ps}\left(d - \gamma c_n\right) + A_s'E_s\frac{\varepsilon_3\left(c_n - d'\right)}{\left(d - c_n\right)}\left(\gamma c_n - d'\right) \quad (42)$$

$$M_n = A_{ps}f_{ps}\left(d - \gamma c_n\right) + A_s'f_y\left(\gamma c_n - d'\right) \quad (43)$$

For a T section or I-section in which the neutral axis falls within the flange, the moment-curvature equations are almost the same as for a rectangular section. The only difference is that the width b is replaced by the width b_f. Therefore, the strand rupture equations for the rectangular section can be

referenced with the change of width. If the neutral axis falls within the web of the component, the moment-curvature equations are as follows.

Eq. (44) is used to determine the neutral axis for a parabolic stress distribution in a T section without mild compression steel.

$$(c_n)^3\left[\left(3\varepsilon_c' + \varepsilon_3\right)f_c' b_w\right] +$$
$$(c_n)^2\left[\left(-3\varepsilon_c' d f_c' b_w + \left(6\varepsilon_c' t_f + 3\varepsilon_3 t_f\right)\right)f_c'\left(b_f - b_w\right) - \frac{3A_{ps}f_{ps}(\varepsilon_c')^2}{\varepsilon_3}\right] +$$
$$c_n\left[\left(-3\varepsilon_c'\left(2dt_f + (t_f)^2\right) - 3\varepsilon_3(t_f)^2\right)f_c'\left(b_f - b_w\right) - \frac{6A_{ps}f_{ps}(\varepsilon_c')^2 d}{\varepsilon_3}\right] +$$
$$\left[\left(3\varepsilon_c'(t_f)^2 d + \varepsilon_3(t_f)^2\right)f_c'\left(b_f - b_w\right) + \frac{3A_{ps}f_{ps}(\varepsilon_c')^2 d^2}{\varepsilon_3}\right] = 0 \quad (44)$$

The neutral axis for a parabolic stress distribution in a T section with mild compression steel that has not yielded is determined using Eq. (45).

$$\left(c_n\right)^3\left[\left(3\varepsilon_c' + \varepsilon_3\right)f_c' b_w\right] + \left(c_n\right)^2\left[\left(-3\varepsilon_c' d f_c' b_w\right.\right.$$
$$\left.\left. + \left(6\varepsilon_c' t_f + 3\varepsilon_3 t_f\right)\right)f_c'\left(b_f - b_w\right) - \frac{3A_{ps}f_{ps}\left(\varepsilon_c'\right)^2}{\varepsilon_3} + 3A_s' E_s\left(\varepsilon_c'\right)^2\right]$$
$$+ c_n\left[\left(-3\varepsilon_c'\left(2dt_f + \left(t_f\right)^2\right) - 3\varepsilon_3\left(t_f\right)^2\right)f_c'\left(b_f - b_w\right)\right.$$
$$\left. - \frac{6A_{ps}f_{ps}\left(\varepsilon_c'\right)^2 d}{\varepsilon_3} - 3A_s' E_s\left(\varepsilon_c'\right)^2\left(d - d'\right)\right]$$
$$+ \left[\left(3\varepsilon_c'\left(t_f\right)^2 d + \varepsilon_3\left(t_f\right)^2\right)f_c'\left(b_f - b_w\right) + \frac{3A_{ps}f_{ps}\left(\varepsilon_c'\right)^2 d^2}{\varepsilon_3}\cdot\right.$$
$$\left. + 3A_s' E_s\left(\varepsilon_c'\right)^2 dd'\right] = 0 \quad (45)$$

Eq. (46) is used to determine the neutral axis for a parabolic stress distribution in a T section with mild compression steel that has yielded:

$$\left(c_n\right)^3\left[\left(3\varepsilon_c' + \varepsilon_3\right)f_c' b_w\right] + \left(c_n\right)^2\left[\left(-3\varepsilon_c' d f_c' b_w\right.\right.$$
$$\left.\left. + \left(6\varepsilon_c' t_f + 3\varepsilon_3 t_f\right)\right)f_c'\left(b_f - b_w\right) - \frac{3\left(A_{ps}f_{ps} - A_s' f_y\right)\left(\varepsilon_c'\right)^2}{\varepsilon_3}\right]$$
$$+ c_n\left[\left(-3\varepsilon_c'\left(2dt_f + \left(t_f\right)^2\right) - 3\varepsilon_3\left(t_f\right)^2\right)f_c'\left(b_f - b_w\right)\right.$$
$$\left. - \frac{6\left(A_{ps}f_{ps} - A_s' f_y\right)\left(\varepsilon_c'\right)^2 d}{\varepsilon_3}\right]$$
$$+ \left[\left(3\varepsilon_c'\left(t_f\right)^2 d + \varepsilon_3\left(t_f\right)^2\right)f_c'\left(b_f - b_w\right)\right.$$
$$\left. + \frac{3\left(A_{ps}f_{ps} - A_s' f_y\right)\left(\varepsilon_c'\right)^2 d^2}{\varepsilon_3}\right] = 0 \quad (46)$$

The curvature is determined from Eq. (40). The corresponding moment for the strand rupture ultimate point is found by summing the moments about the centroid of the tension force.

The ultimate moment for the parabolic stress distribution in a T section without mild compression steel is given by Eq. (47).

$$M_n = \alpha_1 f_c' c_n b_f\left(d - \gamma_1 c_n\right) - \alpha_2 f_c'\left(c_n - t_f\right)\left(b_f - b_w\right)\left(c_n - t_f\right)\left(d - t_f - \gamma_2 c_n\right) \quad (47)$$

Equation (48) is the moment equation for the parabolic stress distribution in a T section with mild compression steel that has not yielded.

$$M_n = \alpha_1 f_c' c_n b_f\left(d - \gamma_1 c_n\right) - \alpha_2 f_c'\left(c_n - t_f\right)\left(b_f - b_w\right)\left(d - t_f - \gamma_2 c_n\right) + A_s' E_s\frac{\varepsilon_3\left(c_n - d'\right)\left(d - d'\right)}{\left(d - c_n\right)} \quad (48)$$

Equation (49) is the final moment equation for the parabolic stress distribution in a T section with mild compression steel that has yielded.

$$M_n = \alpha_1 f_c' c_n b_f\left(d - \gamma_1 c_n\right) - \alpha_2 f_c'\left(c_n - t_f\right)\left(b_f - b_w\right)\left(c_n - t_f\right)\left(d - t_f - \gamma_2 c_n\right) + A_s' f_y\left(d - d'\right) \quad (49)$$

For determining the ultimate point, it is also necessary to determine whether the member will fail due to concrete crushing before the prestressing steel ruptures. For the rectangular cross sections, a concrete crushing failure is more likely due to the reduced concrete compression area, when compared with a T section or I-section. Therefore, initially assume that rectangular sections will fail in concrete crushing.

For a concrete crushing failure, the strain at the extreme concrete compressive fiber is 0.003.[4] As with the yielding point and ultimate point for strand rupture, strain-compatibility analysis is used to determine the ultimate moment and corresponding curvature for concrete crushing. The only difference is that both the tension and the compression force are dependent on the neutral axis location.

The first step is to determine the strain relationships for the various materials. The strain in the prestressing steel due to initial stressing is determined by Eq. (11) and (12); however, the total strain in the prestressing steel cannot be determined until the strain due to the external moment is determined.

Because the failure mode is concrete crushing, the total prestressing strain is not known in advance (unlike the cases of yielding point and strand rupture). Therefore, it is necessary to determine the prestressing strain due to the external moment ε_3 from the strain compatibility as it relates to concrete extreme compression fiber strain. Figure 4 shows the stress and strain distributions for a T or I-section member at a concrete crushing failure. Those distributions are also valid for rectangular sections when the compression block is only in the flange section with C_2 equal to zero.

Referencing Fig. 4, Eq. (50) is used to determine ε_3.

$$\varepsilon_3 = \frac{\varepsilon_{cu}\left(d - c_n\right)}{c_n} \tag{50}$$

where

ε_{cu} = extreme compressive fiber strain at concrete crushing

The strain from the external moment is dependent on the location of the neutral axis. Because the tension force is not known when the mode of failure is concrete crushing, the total strain in the prestressing steel is as follows:

$$\varepsilon_{ps} = \varepsilon_1 + \varepsilon_2 + \frac{\varepsilon_{cu}\left(d - c_n\right)}{c_n}$$

With the total strain ε_{ps} known in terms of depth of the section neutral axis at ultimate strength c_n, the stress in the prestressing steel f_{ps} can be determined in terms of depth of the section neutral axis at ultimate strength c_n. The prestressing strand is assumed to have yielded, and it is either 250 or 270 ksi (1720 or 1860 MPa), low-relaxation, seven-wire strand; these two types of strand have different stress-strain relationships at yielding.[3] For 250 and 270 ksi strands, the prestressing stress after yielding is:

$$f_{ps} = f_{pu} - \frac{0.04}{\varepsilon_1 + \varepsilon_2 + \frac{\varepsilon_{cu}\left(d - c_n\right)}{c_n} - x_1}$$

where

x_1 = constant based on the yield strength of the prestressing strand ($x_1 = 0.0064$ for 250 ksi prestressing strand and $x_1 = 0.0070$ for 270 ksi prestressing strand)

Because the neutral axis is unknown, the prestressing steel tension force is determined in terms of the depth of the section neutral axis at ultimate strength c_n. In addition, tensile force T is not dependent on the concrete cross-section type or the presence of compression mild steel; therefore, Eq. (51) can be used for any of the cross sections considered.

$$T = A_{ps}\left[f_{pu} - \frac{0.04}{\varepsilon_1 + \varepsilon_2 + \frac{\varepsilon_{cu}\left(d - c_n\right)}{c_n} - x_1}\right] \tag{51}$$

The compression force equations are dependent on whether or not there is mild compression steel and the type of concrete cross section. Because the strain at concrete crushing is 0.003, the proportional terms α and α_1 and the neutral axis multipliers γ and γ_1 are known; however, the proportional term α_2 and neutral axis multiplier γ_2 are dependent on the location of the neutral axis.

Equations (52), (53), and (54) are neutral axis equations for the concrete crushing failure mode of a rectangular compression block without mild compression steel, a rectangular compression block with mild compression steel that has not yielded, and a rectangular compression block with mild compression steel that has yielded, respectively.

$$\begin{aligned}&\left[\alpha f'_c b\left(\varepsilon_1 + \varepsilon_2 - \left(\varepsilon_{cu} + x_1\right)\right)\right]\left(c_n\right)^2 \\ &+\left[\alpha f'_c b\varepsilon_{cu} d - f_{pu} A_{ps}\left(\varepsilon_1 + \varepsilon_2 - \left(\varepsilon_{cu} + x_1\right)\right) + 0.04 A_{ps}\right]c_n \\ &- f_{pu} A_{ps} d\varepsilon_{cu} = 0\end{aligned} \tag{52}$$

$$\begin{aligned}&\left[\alpha f'_c b\left(\varepsilon_1 + \varepsilon_2 - \left(\varepsilon_{cu} + x_1\right)\right)\right]\left(c_n\right)^3 \\ &+\left[\alpha f'_c b\varepsilon_{cu} d - f_{pu} A_{ps}\left(\varepsilon_1 + \varepsilon_2 - \left(\varepsilon_{cu} + x_1\right)\right) + 0.04 A_{ps}\right. \\ &\left. + A'_s E_s \varepsilon_{cu}\left(\varepsilon_1 + \varepsilon_2 - \left(\varepsilon_{cu} + x_1\right)\right)\right]\left(c_n\right)^2 \\ &+\left[-f_{pu} A_{ps} d\varepsilon_{cu} + A'_s E_s\left(\varepsilon_{cu}\right)^2 d - A'_s E_s d'\varepsilon_{cu}\left(\varepsilon_1 + \varepsilon_2 - \left(\varepsilon_{cu} + x_1\right)\right)\right]c_n \\ &- A'_s E_s\left(\varepsilon_{cu}\right)^2 d'd = 0\end{aligned} \tag{53}$$

$$\begin{aligned}&\left[\alpha f'_c b\left(\varepsilon_1 + \varepsilon_2 - \left(\varepsilon_{cu} + x_1\right)\right)\right]\left(c_n\right)^2 + \\ &\left[\alpha f'_c b\varepsilon_{cu} d - f_{pu} A_{ps}\left(\varepsilon_1 + \varepsilon_2 - \left(\varepsilon_{cu} + x_1\right)\right)\right. \\ &\left. + 0.04 A_{ps} + A'_s f_y\left(\varepsilon_1 + \varepsilon_2 - \left(\varepsilon_{cu} + x_1\right)\right)\right]c_n \\ &-\left(f_{pu} A_{ps} d\varepsilon_{cu} - A'_s E_s \varepsilon_{cu} d\right) = 0\end{aligned} \tag{54}$$

After the neutral axis is determined, the curvature and the corresponding moment can be determined. The curvature is found from Eq. (55).

$$\phi_n = \frac{\varepsilon_{cu}}{c_n} = \frac{0.003}{c_n} \tag{55}$$

The corresponding moment for the ultimate point is found by summing the moments about the centroid of the concrete compressive force. Equations (56), (57), and (58) determine the ultimate moment for a rectangular compression block without mild compression steel, a rectangular compression block with non-yielded mild compression steel, and a rectangular compression block with yielded mild compression steel, respectively.

$$M_n = A_{ps}\left[f_{pu} - \frac{0.04}{\varepsilon_1 + \varepsilon_2 + \frac{\varepsilon_{cu}\left(d - c_n\right)}{c_n} - x_1}\right]\left(d - \gamma c_n\right) \tag{56}$$

$$M_n = A_{ps}\left[f_{pu} - \frac{0.04}{\varepsilon_1 + \varepsilon_2 + \frac{\varepsilon_{cu}\left(d - c_n\right)}{c_n} - x_1}\right]\left(d - \gamma c_n\right) + A_s' E_s \frac{\varepsilon_{cu}\left(c_n - d'\right)}{c_n}\left(\gamma c_n - d'\right) \quad (57)$$

$$M_n = A_{ps}\left[f_{pu} - \frac{0.04}{\varepsilon_1 + \varepsilon_2 + \frac{\varepsilon_{cu}\left(d - c_n\right)}{c_n} - x_1}\right]\left(d - \gamma c_n\right) + A_s' f_y\left(\gamma c_n - d'\right) \quad (58)$$

Because the flange of a T section or I-section is relatively wide, the concrete crushing failure mode is less likely to control the ultimate capacity in these types of sections (compared with a rectangular section). Therefore, the derivation of the moment–curvature equations for T section and I-section components in a concrete crushing failure mode is not discussed here.

Structural response (load-deflection behavior)

The structural response for the component is determined after the four points that define the trilinear moment-curvature relationship for the particular cross section are established. The response is determined using the first and second moment-area theorems. The first theorem validates that the curvature, at any point, is equal to the ordinate M/EI, where M is the moment, E is the modulus of elasticity, and I is the moment of inertia. The second theorem is then used to find the maximum deflection at midspan. Figure 2 illustrates the trilinear moment-curvature behavior of a prestressed concrete beam.

The effective flexural rigidity of the section reduces with increased moment. The beam is divided into three general regions: uncracked, postcracked, and postyielding. The uncracked region is terminated by the external moment required to cause the tension stress f_r in the bottom extreme concrete fiber. The postcracked region is bounded by the first cracked boundary point and an external moment that causes the prestressing strand to yield, at 0.01 strain. The postyielding region is bounded by the first yielding boundary point and the external moment required for the member to fail, by strand rupture or concrete crushing. Each of the boundary moments has a corresponding curvature: uncracked region, postcracked region, and postyielding region, as defined by Eq. (59), (60), and (61), respectively.

$$\phi_a = \frac{\left(M_a\right)}{\left(M_{cr}\right)}\left(\phi_{cr} - \phi_{in}\right) + \phi_{in} \quad (59)$$

$$\phi_a = \frac{\left(M_a - M_{cr}\right)}{\left(M_y - M_{cr}\right)}\left(\phi_y - \phi_{cr}\right) + \phi_{cr} \quad (60)$$

$$\phi_a = \frac{\left(M_a - M_y\right)}{\left(M_n - M_y\right)}\left(\phi_n - \phi_y\right) + \phi_y \quad (61)$$

where

ϕ_a = curvature corresponding to the maximum moment

The locations and sizes of the regions depend on the level and type of applied load. This formulation furnishes closed-form expressions for midspan deflection $\Delta_{midspan}$ of simple beams under four-point bending and uniformly distributed load. The general solution can be obtained by adding the deflection contribution of the three regions, as shown in Eq. (62).

$$\Delta_{midspan} = \delta_1 + \delta_2 + \delta_3 = \int_0^{L_g} x\phi_{un}\left(x\right)dx + \int_{L_g}^{L_y} x\phi_{pc}\left(x\right)dx + \int_{L_y}^{\frac{L}{2}} x\phi_{py}\left(x\right)dx \quad (62)$$

where

ϕ_{un} = uncracked curvature

ϕ_{pc} = postcracked curvature

ϕ_{py} = postyielding curvature

Four-point bending The four-point bending loading condition is characterized by two equal point loads placed symmetrically on the beam. **Figure 5** shows this condition for half of the beam.

The four-point bending loading condition simplifies load-deflection analysis because the moment increases linearly from the beam support to the application point of the force and moments remain constant between loading points. Applying the trilinear moment-curvature response to the beam, the curvature distribution within each flexural stiffness region is linear. Regular shapes, such as triangles and rectangles, constitute the areas under the moment-curvature diagram. The

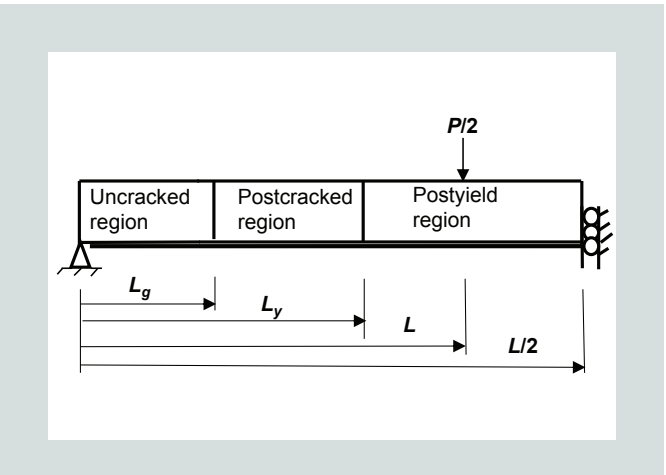

Figure 5. Profile of a half beam showing the three distinct regions.
Note: L = span length; L_a = length from the support to the load application point; L_g = length from the support to the cracking moment location (uncracked region); L_y = length from the support to the yield moment location; P = point load.

regular shapes allow for closed-form expressions for midspan deflections to be obtained. These expressions are determined by summing the moment of the areas under the curve relative to the end point, and their derivations depend upon the moment at the load application point. Equation (63) gives the moment at the point of load application M_a.

$$M_a = \frac{PL_a}{2} \tag{63}$$

where

P = point load

L_a = length from the support to the load application point

The deflection expressions are separated into three scenarios: the uncracked region where $M_a \le M_{cr}$; the postcracked region where $M_{cr} < M_a \le M_y$; and the postyielding region where $M_y < M_a \le M_n$. These scenarios are denoted by the flexural stiffness region where the moment at load application M_a lies. Therefore, the uncracked, postcracked, and postyielding regions are used to indicate the deformation progression. **Figure 6** shows the curvature distribution for the uncracked, postcracked, and postyielding scenarios for the four-point bending case.

After curvatures are determined for the uncracked scenario (Fig. 6), the first region can be represented by the classical uncracked beam problem, producing a midspan deflection described by (Eq. [64]).

$$\Delta_{midspan} = \frac{\phi_{in}}{6}\left(L_a\right)^2 + \frac{\phi_a}{24}\left(3L^2 - 4\left(L_a\right)^2\right) \tag{64}$$

where

ϕ_a = curvature corresponding to the maximum moment $= \frac{M_a}{M_{cr}}\left(\phi_{cr} - \phi_{in}\right) + \phi_{in}$

M_a = applied moment $= \frac{PL_a}{2}$

E_c = modulus of elasticity of concrete = $57{,}000\sqrt{f'_c}$ with $\sqrt{f'_c}$ in psi or = $4700\sqrt{f'_c}$ with $\sqrt{f'_c}$ in MPa

L_a = length from the support to the load application point (shear span)

L = beam span

The deflection Eq. (64) is valid if M_a is less than the cracking moment M_{cr}. If the beam is unloaded, the curvature corre-

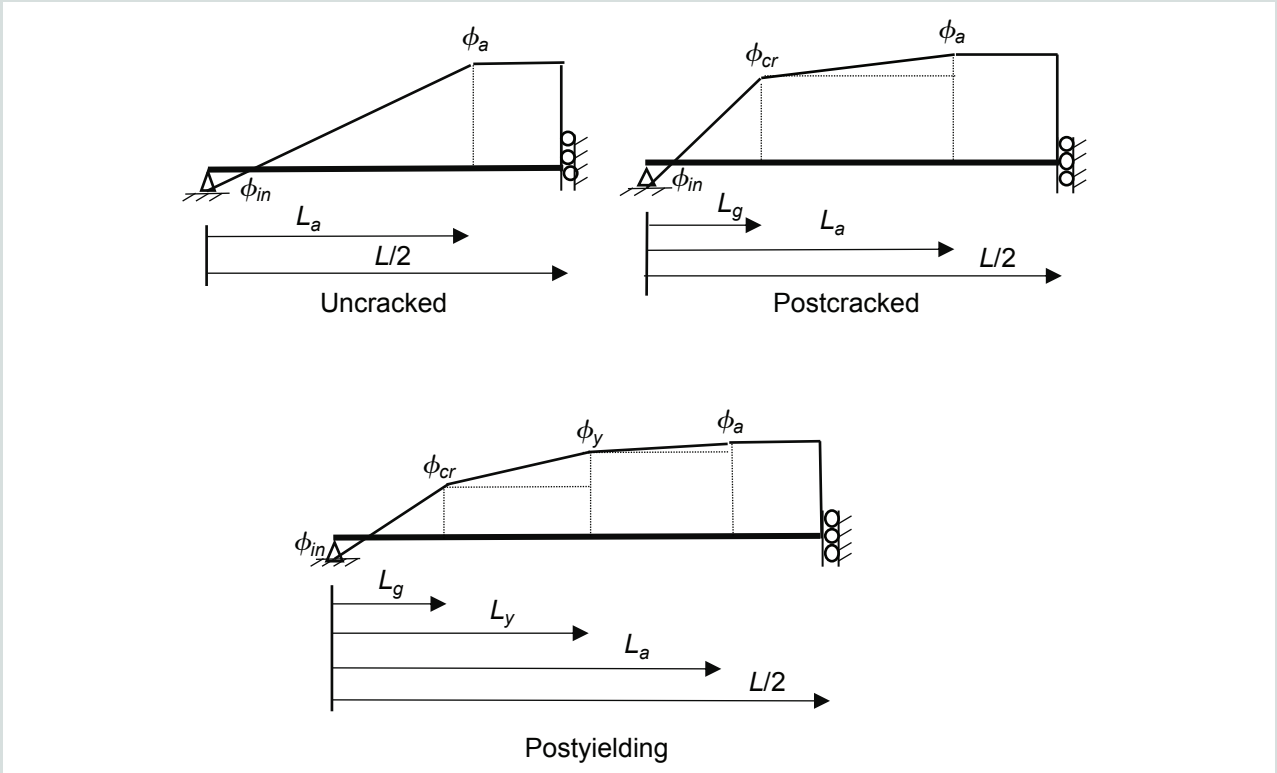

Figure 6. Curvature distribution for the uncracked scenario, postcracked scenario, and postyielding scenario for the four-point bending case.
Note: L = span length; L_a = length from the support to the load application point; L_g = length from the support to the cracking moment location (uncracked region); L_y = length from the support to the yield moment location; ϕ_a = curvature at the point of load application; ϕ_{cr} = curvature at the cracking moment location; ϕ_{in} = initial curvature; ϕ_y = yield point curvature.

sponding to the maximum moment ϕ_a equals the initial curvature ϕ_{in}, and the maximum initial camber is obtained.

For the postcracked scenario, three curvature points define the moment-curvature response (Fig. 6), with the extent of the cracking region defined as L_g (Eq. [65]).

$$L_g = \frac{2M_{cr}}{P} \tag{65}$$

where

M_{cr} = $\left[\frac{\left(f_r A_{gt} + P_e\right)e^2}{y_t}\right] + P_e e$

f_r = modulus of rupture according to ACI 318-19

y_t = distance between the neutral axis of the uncracked transformed section to the extreme fiber in tension

The midspan deflection is determined using the moment-area theorem by analytical integration of the moment of curvature distribution along half the span about the hinge support (Eq. [66]).

$$\Delta_{midspan} = \int_0^{\frac{L}{2}} x\phi(x)\,dx = \int_0^{L_g} x\phi_{un}(x)\,dx + \int_{L_g}^{L_a} x\phi_{pc}(x)\,dx + \int_{L_a}^{\frac{L}{2}} x\phi_a\,dx \tag{66}$$

where

$\phi(x)$ = generic curvature expression for a beam

$\phi_{pc}(x)$ = curvature expression for the postcracked region

ϕ_a = maximum curvature for the constant moment region

The uncracked curvature ϕ_{un} is defined in Eq. (67) and the postcracked curvature ϕ_{pc} is defined in Eq. (68).

$$\phi_{un}(x) = \phi_{in} + \frac{M(x)}{M_{cr}}\left(\phi_{cr} - \phi_{in}\right) \tag{67}$$

where

$M(x)$ = moment expression as a function of x

$$\phi_{pc}(x) = \phi_{cr} + \frac{M(x) - M_{cr}}{M_y - M_{cr}}\left(\phi_y - \phi_{cr}\right) \tag{68}$$

To solve the integration, triangular and rectangular areas are used to find the moment area under the curvature diagram at the postyielding stage in closed form (Fig. 6). This leads to a midspan deflection equation (Eq. [69]) that is valid if the applied moment is less than or equal to the yielding moment.

$$\Delta_{midspan} = \frac{\phi_{in}}{6}\left(L_a\right)^2 + \frac{\phi_a}{24}\left(3L^2 - 4\left(L_a\right)^2\right) + \frac{\left(L_a + L_g\right)}{6}\left(\phi_{cr}L_a - \phi_a L_g\right) \tag{69}$$

In Eq. (69), maximum curvature for the constant moment region ϕ_a is calculated by linear interpolation between the cracking curvature ϕ_{cr} and the yielding curvature ϕ_y, as shown in Fig. 6 and given by Eq. (60).

In the postyielding scenario, four curvatures define the moment-curvature response (Fig. 6). Upon yielding of the prestressing steel (tension), sections in the postyielding stage are assumed to be fully cracked. The moments and their corresponding curvatures are previously defined, except for M_n and ϕ_n. The location of the cracking moment is determined from Eq. (65), and the location of the yielding moment is determined from Eq. (70).

$$L_y = \frac{2M_y}{P} \tag{70}$$

The midspan deflection in terms of the curvatures and their locations yields Eq. (71).

$$\Delta_{midspan} = \int_0^{L_g} x\phi_{un}(x)dx + \int_{L_g}^{L_y} x\phi_{pc}(x)\,dx + \int_{L_y}^{L_a} x\phi_{py}(x)\,dx + \int_{L_a}^{\frac{L}{2}} x\phi_a\,dx \tag{71}$$

where

$\phi_{py}(x)$ = curvature expression for the postyielding region

The uncracked curvature ϕ_{un} is defined in Eq. (67); the postcracked-to-yield curvature ϕ_{pc} is defined in Eq. (68); and the postyielding-to-nominal (ultimate) curvature ϕ_{py} is defined in Eq. (72).

$$\phi_{py} = \phi_y + \frac{M(x) - M_y}{M_n - M_y}\left(\phi_n - \phi_y\right) \tag{72}$$

In addition, ϕ_a is calculated by linear interpolation between the yielding curvature ϕ_y and the ultimate curvature as shown in Fig. 6 and given by Eq. (61).

M_y is calculated by Eq. (26), (27), (34), (35), or (36), depending on section shape and compression mild steel condition; ϕ_y is calculated by Eq. (21); M_n is calculated by Eq. (56), (57), or (58), depending on section shape and compression mild steel condition; ϕ_n is calculated from Eq. (55). Equation (73) can be used as the general equation to calculate midspan deflection of simple beams subjected to four-point bending. In this case, L_y equals L_a and ϕ_y equals ϕ_a may be substituted to show this reduction.

$$\Delta_{midspan} = \frac{\phi_{in}\left(L_g\right)^2}{6} + \frac{\phi_a}{24}\left(3L^2 - 4\left(L_a\right)^2\right) + \frac{\phi_{cr}L_y - \phi_y L_g}{6}\left(L_g + L_y\right) + \frac{\phi_y L_a - \phi_a L_y}{6}\left(L_a + L_y\right) \tag{73}$$

Uniform loading While the four-point bending condition provides a simple loading case for a deflection analysis, the

use of four-point bending is typically limited to laboratory tests. A more common loading case is uniform loading, which is also a symmetric loading case. The uniform loading case is characterized by a load w distributed evenly across the component. Moment-area theorem is used to determine the deflection at midspan. Because the load is distributed across the entire beam evenly, the moment distribution is not linear. Therefore, when the trilinear moment-curvature relationship is applied to a component, the curvature distribution is parabolic in each region. **Figure 7** shows the curvature distribution for a uniform loading condition.

The curvature distribution corresponding to the parabolic moment diagram of the uniform load case is determined by integration in closed form. The solution is obtained by adding the deflection contribution of the three regions (Eq. [66]).

The moment along half of the beam is given by Eq. (74).

$$M = \frac{wL}{2}x - \frac{wx^2}{2} \tag{74}$$

For deflection at the uncracked stage, M_{cr} and L_g can be substituted in Eq. (74) for M and x, respectively, and the equation can be solved for L_g (Eq. [75]).

$$L_g = \frac{L}{2} - \frac{L}{2}\sqrt{1 - \frac{8M_{cr}}{wL^2}} \tag{75}$$

With the location of the cracking moment found, the deflection contribution of the uncracked region is determined. The first integral of Eq. (62) produces Eq. (76).

$$\delta_1 = \frac{w\left(L_g\right)^3\left(\phi_{cr} - \phi_{in}\right)}{2M_{cr}}\left(\frac{L}{3} - \frac{L_g}{4}\right) + \frac{\phi_{in}\left(L_g\right)^2}{2} \tag{76}$$

If the member has not cracked, $L/2$ is substituted for L_g in Eq. (76) and simplified to Eq. (77).

$$\Delta_{midspan} = \frac{5wL^4\left(\phi_{cr} - \phi_{in}\right)}{384M_{cr}} + \frac{\phi_{in}L^2}{8} = \frac{5wL^4}{384E_cI_{gt}} + \frac{P_eeL^2}{8E_cI_{gt}} \tag{77}$$

Similar to the cracking point, the yielding moment location is determined from Eq. (78). If the terms M_y and L_y are substituted for M and x, respectively, in Eq. (74), the location where the first yield occurs along the length of the member can be calculated by Eq. (79).

$$M_y = \frac{wL}{2}L_y - \frac{w\left(L_y\right)^2}{2} \tag{78}$$

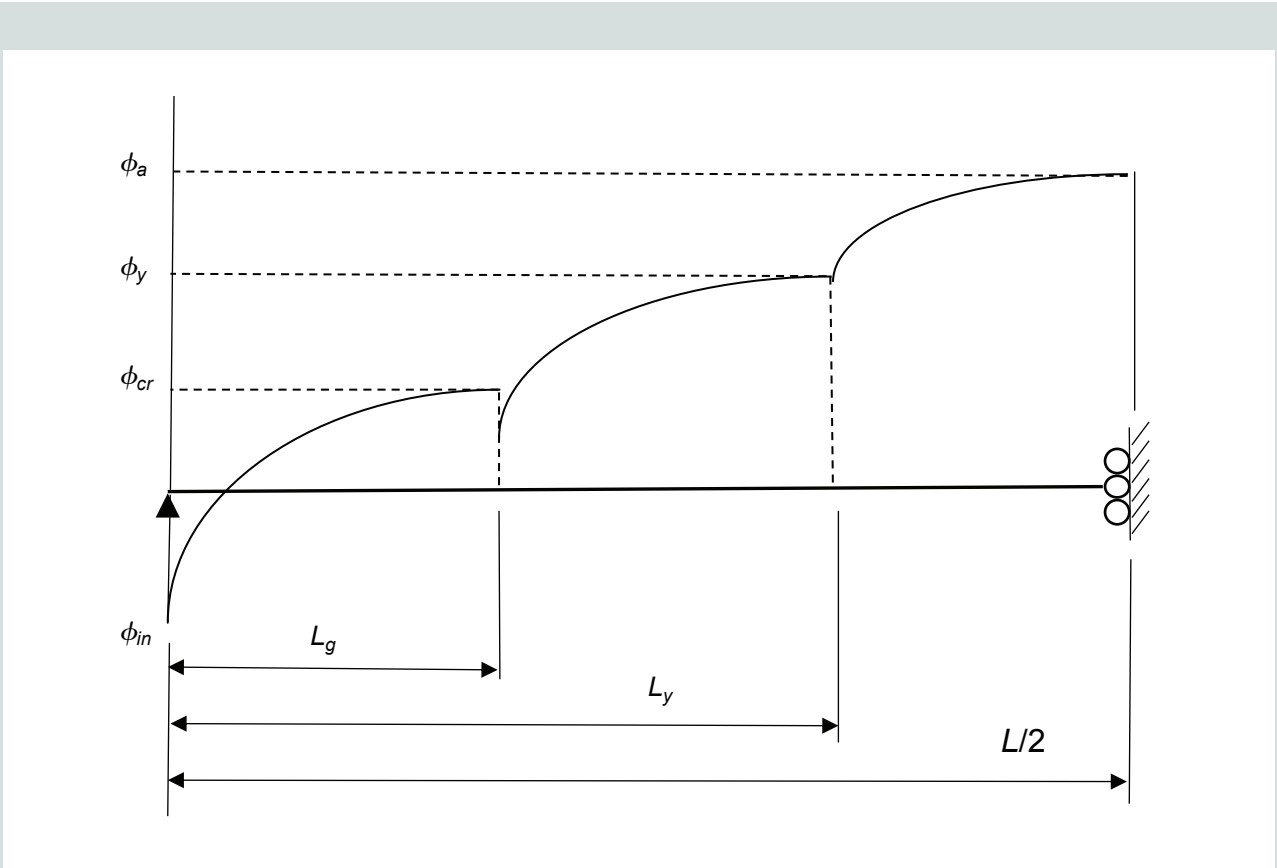

Figure 7. Curvature distribution for uniform loading condition for the half span.
Note: L = span length; L_g = length from the support to the cracking moment location (uncracked region); L_y = length from the support to the yield moment location; ϕ_a = curvature at the point of load application; ϕ_{cr} = curvature at the cracking moment location; ϕ_{in} = initial curvature; ϕ_y = yield point curvature.

$$L_y = \frac{L}{2} - \frac{L}{2}\sqrt{1 - \frac{8M_y}{wL^2}} \tag{79}$$

In addition to determining the location of the first yielding point, Eq. (60) is used to determine the postcracked flexural stiffness region in the curvature distribution. The deflection contribution for the postcracked flexural stiffness region represented by Eq. (80) is derived by substituting Eq. (74) and Eq. (60) into the second term of Eq. (62) and simplifying.

$$\delta_2 = \frac{\left(\phi_y - \phi_{cr}\right)}{\left(M_y - M_{cr}\right)}\left[\frac{w\left(L_y\right)^3}{2}\left(\frac{L}{3} - \frac{L_y}{4}\right) + \frac{M_{cr}\left(\left(L_g\right)^2 - \left(L_y\right)^2\right)}{2} - \frac{w\left(L_g\right)^3}{2}\left(\frac{L}{3} - \frac{L_g}{4}\right)\right] + \frac{\phi_{cr}\left(\left(L_y\right)^2 - \left(L_g\right)^2\right)}{2} \tag{80}$$

For the postyielding flexural stiffness region, the curvature distribution is determined by Eq. (61). The maximum moment M_a is located at $L/2$ due to the symmetric loading condition and simply supported end condition. Therefore, if the member has not reached the postyielding flexural stiffness region, the contribution of the postcracked flexural stiffness region is determined by substituting $L/2$ for L_y in Eq. (80) to yield Eq. (81).

$$\delta_2 = \frac{\left(\phi_y - \phi_{cr}\right)}{\left(M_y - M_{cr}\right)}\left[\frac{5wL^4}{384} + \frac{M_{cr}}{2}\left(\left(L_g\right)^2 - \frac{L^2}{4}\right) - \frac{w\left(L_g\right)^3}{2}\left(\frac{L}{3} - \frac{L_g}{4}\right)\right] + \frac{\phi_{cr}}{2}\left(\frac{L^2}{4} - \left(L_g\right)^2\right) \tag{81}$$

Then, to determine the total deflection of the member, Eq. (76) and (81) are added together to yield Eq. (82).

$$\Delta_{midspan} = \frac{w\left(L_g\right)^3\left(\phi_{cr} - \phi_{in}\right)}{2M_{cr}}\left(\frac{L}{3} - \frac{L_g}{4}\right) + \frac{\phi_{in}\left(L_g\right)^2}{2} + \frac{\left(\phi_y - \phi_{cr}\right)}{\left(M_y - M_{cr}\right)}\left[\frac{5wL^4}{384} + \frac{M_{cr}}{2}\left(\left(L_g\right)^2 - \frac{L^2}{4}\right) - \frac{w\left(L_g\right)^3}{2}\left(\frac{L}{3} - \frac{L_g}{4}\right)\right] + \frac{\phi_{cr}}{2}\left(\frac{L^2}{4} - \left(L_g\right)^2\right) \tag{82}$$

Substituting Eq. (78) and Eq. (61) into the third term of Eq. (71) creates Eq. (83), which gives the deflection contribution of the postyielding flexural stiffness region.

$$\delta_3 = \frac{\left(\phi_n - \phi_y\right)}{\left(M_n - M_y\right)}\left[\frac{5wL^4}{384} + \frac{M_y}{2}\left(\left(L_y\right)^2 - \frac{L^2}{4}\right) - \frac{w\left(L_y\right)^3}{2}\left(\frac{L}{3} - \frac{L_y}{4}\right)\right] + \frac{\phi_y}{2}\left(\frac{L^2}{4} - \left(L_y\right)^2\right) \tag{83}$$

Equation (84) determines the deflection at midspan of a beam that has a postyielding region. This equation is produced by inserting Eq. (76), (80), and (83) into Eq. (62) for the first, second, and third terms, respectively.

$$\Delta_{midspan} = \delta_1 + \delta_2 + \delta_3 = \frac{wL_g{}^3\left(\phi_{cr} - \phi_{in}\right)}{2M_{cr}}\left(\frac{L}{3} - \frac{L_g}{4}\right) + \frac{\left(\phi_y - \phi_{cr}\right)}{\left(M_y - M_{cr}\right)}\left[\frac{wL_y{}^3}{2}\left(\frac{L}{3} - \frac{L_y}{4}\right) + \frac{M_{cr}\left(L_g{}^2 - L_y{}^2\right)}{2} - \frac{wL_g{}^3}{2}\left(\frac{L}{3} - \frac{L_g}{4}\right)\right] + \frac{\phi_{cr}\left(L_y{}^2 - L_g{}^2\right)}{2} + \frac{\left(\phi_n - \phi_y\right)}{\left(M_n - M_y\right)}\left[\frac{5xL^4}{384} + \frac{M_y}{2}\left(L_y^2 - \frac{L^2}{4}\right) - \frac{wL_y^3}{2}\left(\frac{L}{3} - \frac{L_y}{4}\right)\right] + \frac{\phi_y}{2}\left(\frac{L^2}{4} - L_y^2\right) \tag{84}$$

Comparisons of predictions and experimental results

The proposed trilinear method was checked against data from investigations of six prestressed concrete specimens, including some that have moment-curvature comparisons, some that have load-deflection comparisons, and some that have both. The specimens were rectangular or T-shaped sections with or without mild compression steel and were tested in three- and four-point bending and uniform loading.

Beams tested by Warwaruk et al.

Warwaruk et al.[9] conducted extensive experimental work, 82 rectangular prestressed concrete beams, at the University of Illinois in the early 1960s. These tests included bonded, unbonded, and partially bonded beams. The major variables involved were: the amount of reinforcement (0.10 to 0.95%), the concrete strength (1270 to 8320 psi, 8.8 to 57.4 MPa), the effective prestress (20,000 to 150,000 psi, 138 to 1034 MPa), and the loading (midspan and two equals loads at third points of the span). Warwaruk[10] used specimens from Warwaruk et al.[9] to presented moment-curvature and load-deflection experimental data on prestressed concrete beams. In addition, Burns[11] used the Warwaruk et al.[9] test specimens to provide the stress-strain relationship, which matches closely to the PCI[3] bilinear approximation, for the prestressing strand used. These three manuscripts presented similar data; the selected specimens are shown in **Table 1**.

Figure 8 shows the moment-curvature curves for beam 1 presented in Warwaruk et al.[9] and Warwaruk[10] and the proposed trilinear method accurately represents the moment-curvature graph (shown by the solid, blue line with diamonds) of the test specimens. In addition, **Fig. 9** shows that results from the proposed method correlate well with the experimental data in the linear elastic, postcracked, and postyielding regions. The major difference is that the ultimate curvature, shown in

Table 1. Specimen data from Warwaruk et al.

Beam mark	Height, in.	Width, in.	Prestressing depth, in.	f'_c, psi	f_{se}, ksi	A_{ps}, in.^{2}
1	12	6	9	5280	118	0.091
2	12	6	9	3970	114	0.211
3	12	6	9	5230	112	0.362

Source: Data from Warwaruk et al. (1962).

Note: A_{ps} = area of prestressing steel; f'_c = design compressive strength of concrete; f_{se} = initial tensioning stress in the prestressing steel after losses. 1 in. = 25.4 mm; 1 in.2 = 654.2 mm2; 1 psi = 6.895 kPa; 1 ksi = 6.895 MPa.

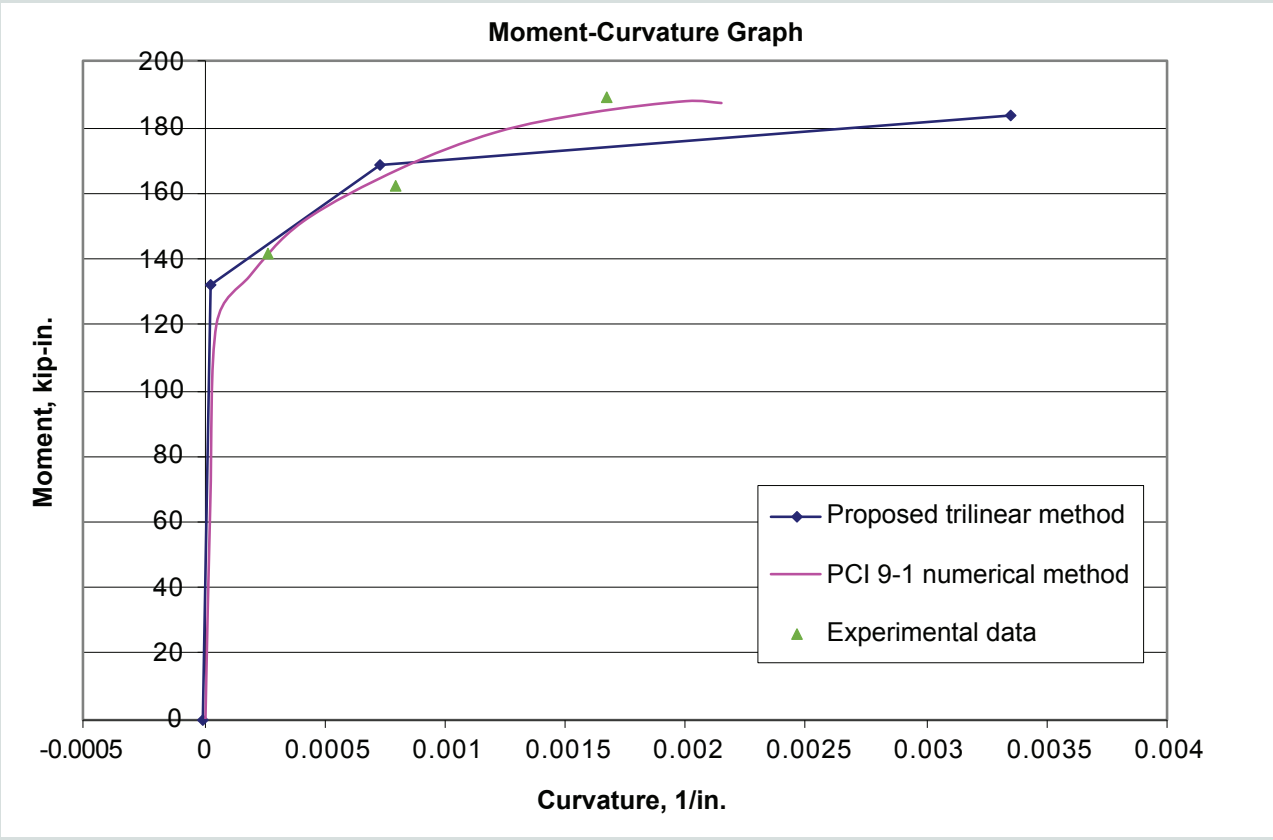

Figure 8. Moment-curvature graph for beam 1 in Burns and Warwaruk.
Sources: Data from Burns (1964) and Warwaruk (1965).
Note: PCI 9-1 numerical method = numerical analysis results presented in Burns. 1 in. = 25.4 mm; 1 kip-in. = 0.113 kN-m.

Fig. 8, and the corresponding ultimate deflection, shown in Fig. 9 as the solid blue line with diamonds, predicted by the proposed method are larger than the experimental (shown by the solid green line) and numerical analysis results (shown by solid pink line with squares) presented in Burns[11] in Fig. 8 and Warwaruk[10] in Fig. 9. The larger deflection prediction is a direct result of the larger ultimate curvature. The larger ultimate curvature can be attributed to the use of actual curvature at the center of the span calculated in the presented procedure instead of the average curvature as presented by Burns.[11]

Compared with beam 1, the area of prestressing in beam 2 was increased to 0.211 in.^{2} (136 mm^2), while the rest of the beam parameters for these two specimens were relatively consistent.[9] This increase in prestressing steel increased the ultimate moment capacity and reduced the maximum curvature of beam 2; also shown in Burns'[11] results. The increase in ultimate moment capacity and reduction in maximum curvature were due to the increase in tension force and the lowering of the neutral axis at the failure moment. **Figure 10** shows that the proposed trilinear method (shown by the solid blue line with diamonds) correlates well with the numerical analysis results (shown by solid pink line with squares) presented in Burns[11]; however, **Fig. 11** shows a significant difference between the numerical analysis results (shown by solid pink line with squares) presented in Warwaruk[10] and experimental (shown by the solid

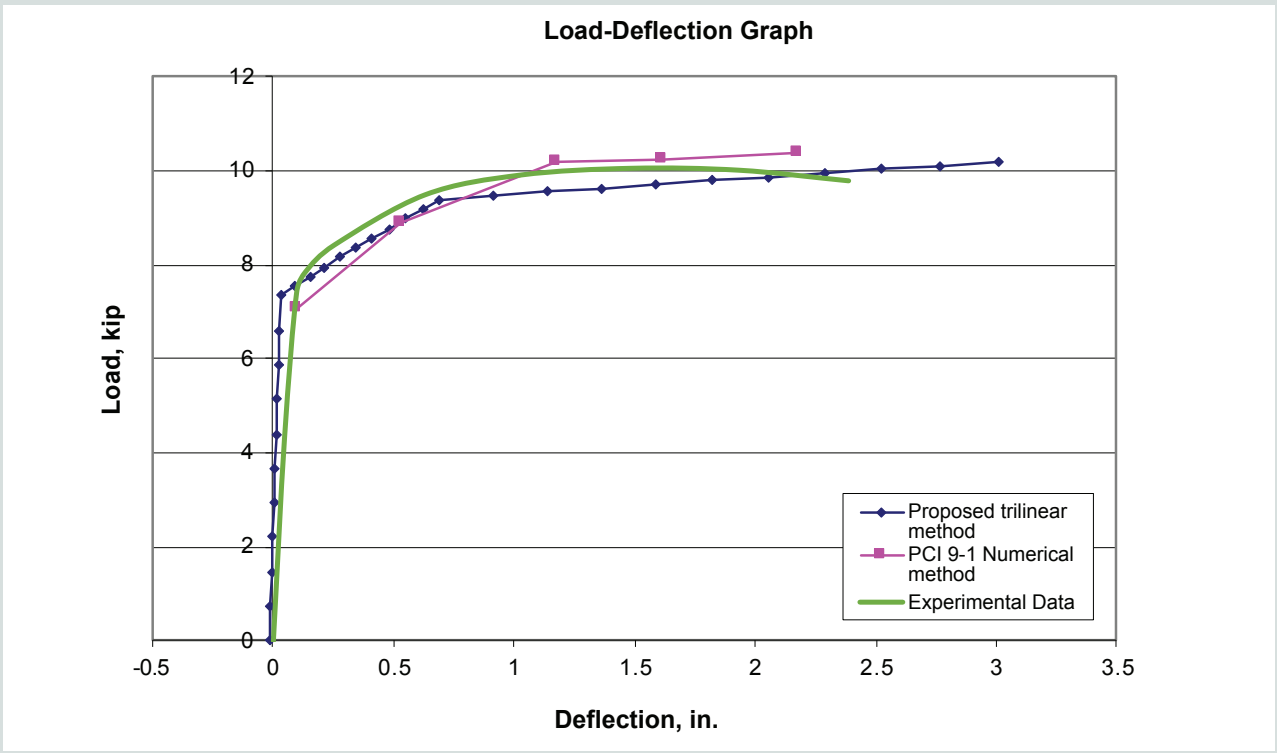

Figure 9. Load-deflection graph for beam 1 in Burns and Warwaruk.
Sources: Data from Burns (1964) and Warwaruk (1965).
Note: PCI 9-1 numerical method = numerical analysis results presented in Warwaruk. 1 in. = 25.4 mm; 1 kip = 4.448 kN.

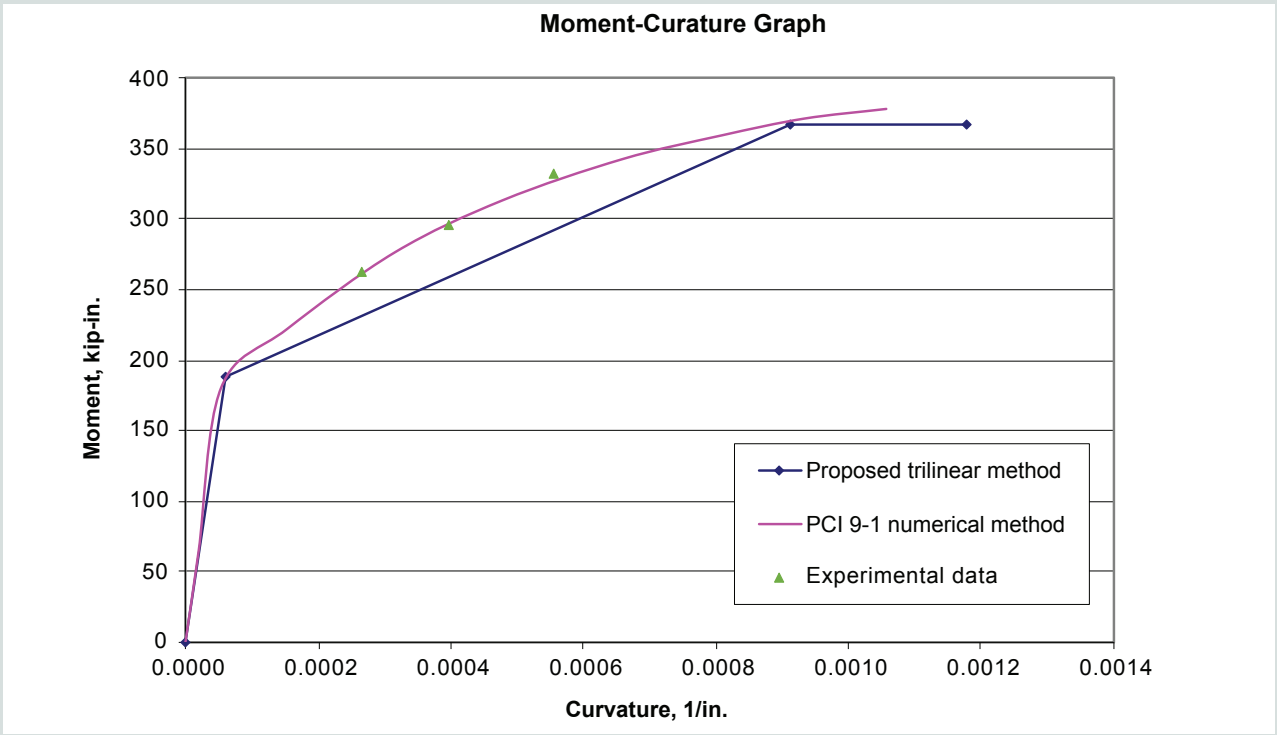

Figure 10. Moment-curvature graph for beam 2 in Burns and Warwaruk.
Sources: Data from Burns (1964) and Warwaruk (1965).
Note: PCI 9-1 numerical method = numerical analysis results presented in Burns. 1 in. = 25.4 mm; 1 kip-in. = 0.113 kN-m.

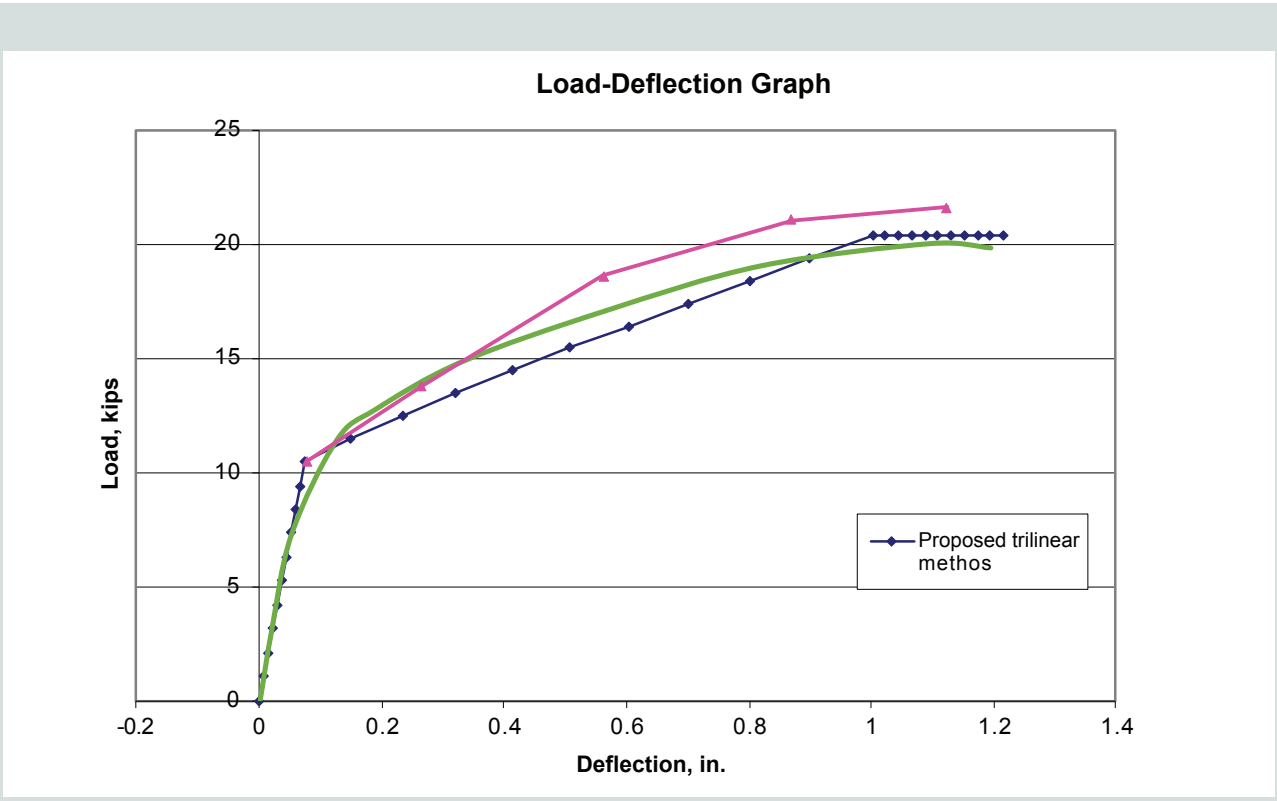

Figure 11. Load-deflection graph for beam 2 in Burns and Warwaruk.
Sources: Data from Burns (1964) and Warwaruk (1965).
Note: PCI 9-1 numerical method = numerical analysis results presented in Burns. 1 in. = 25.4 mm; 1 kip = 4.448 kN.

green line) moment-curvature curves and the proposed method in the postcracked region. This difference is due to the use of a simplified trilinear relationship to represent the moment-curvature in the proposed method. Nevertheless, the proposed procedure yields conservative results. Figure 11 shows that for deflection calculations, the discrepancy caused by using a trilinear moment-curvature response is minor.

The area of prestressing steel in beam 3 was 0.362 in.^{2} (234 mm^2).[9] Compared with beam 2, the ultimate moment capacity increased and the maximum curvature decrease. However, due to the increase in prestressing steel, the beam reached the ultimate moment stage prior to strand yielding, at a strand strain of 0.0088. As a result, the proposed trilinear response curve of the moment-curvature and load-deflection responses show no yielding plateau. This case represents a brittle failure due to the attainment of concrete crushing prior to strand yielding driven by the high strand area used in this beam specimen.

Figures 12 and **13** show good correlation between the proposed trilinear method (shown by the solid, blue line with diamonds) and the experimental (shown by the solid green line) and the numerical analysis results (shown by solid pink line with squares) presented in Burns[11] in Fig. 12 and Warwaruk[10] in Fig. 13. The major discrepancy is due to the use of the trilinear curve for the moment-curvature response in the proposed method. The discrepancy is reflected in Fig. 13 but the proposed trilinear curve still closely reproduces the moment-curvature curve from previous studies[9,10,11] however, because the magnitude of the discrepancy is small, the proposed method still gives accurate and conservative deflection predictions.

As with beams 1 and 2, the moment-curvature curve for the proposed method was artificially zeroed for beam 3. Because the yielding plateau of the moment-curvature response descends slightly, adjustments were also made to the deflection calculations in the proposed method - the location of the yielding point and cracking point were held constant after yielding point reach the point of load application. In addition, the curvature for the shear region of beam 3 was allowed to increase linearly to the ultimate curvature as the moment decreased. The changes allowed the load-deflection response to capture both the increased deflection and the release of the load. Therefore, the load-deflection response has a descending yielding plateau.

Beams tested by Paranagama and Edwards

Paranagama and Edwards[12] studied the response of prestressed beams to cyclic loading along with one control beam for each underreinforced, overreinforced, and balanced condition. For this study, we compared data for the statically loaded control beams A1 (balanced condition) and B1 (underreinforced condition) to predictions from the proposed trilinear method. The specimen data from Paranagama and Edwards are presented in **Table 2**. The loading setup was a single point load in the middle of the beam, three-point bending; however, Paranagama and Edwards[12] only provided

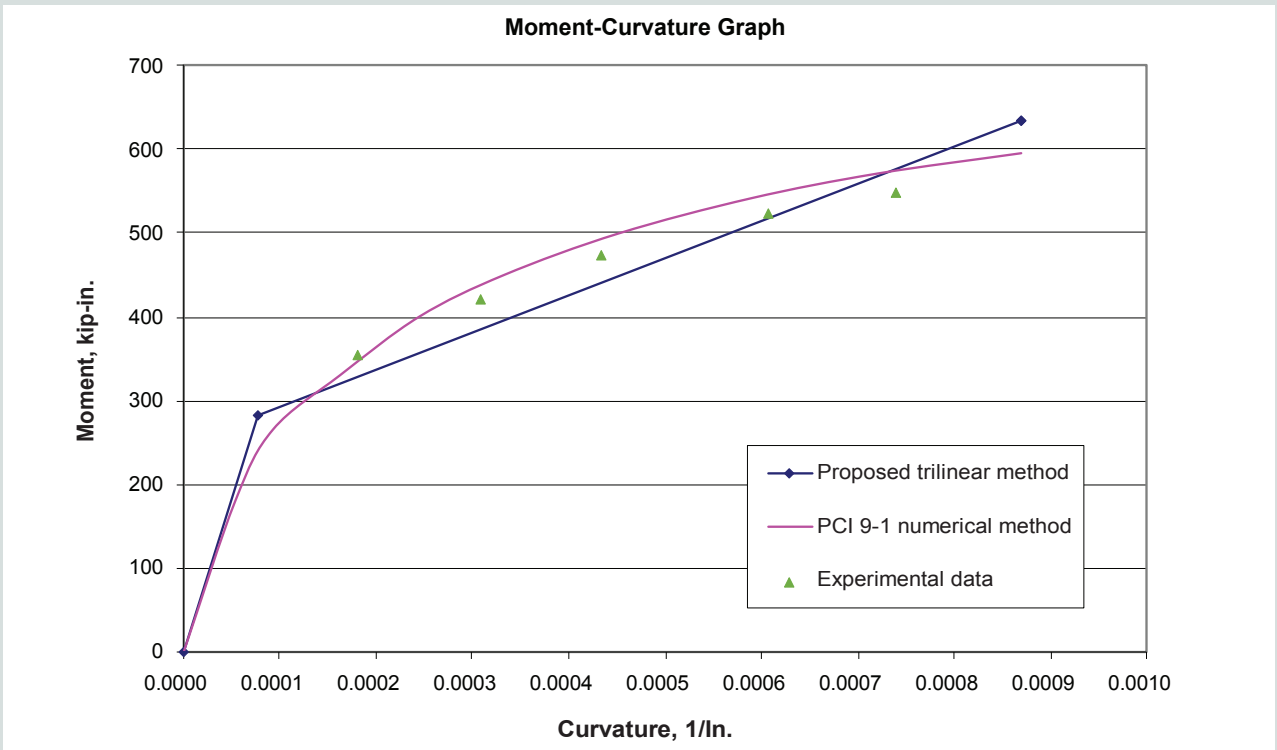

Figure 12. Moment-curvature graph for beam 3 in Burns and Warwaruk.
Sources: Data from Burns (1964) and Warwaruk (1965).
Note: PCI 9-1 numerical method = numerical analysis results presented in Burns. 1 in. = 25.4 mm; 1 kip-in. = 0.113 kN-m.

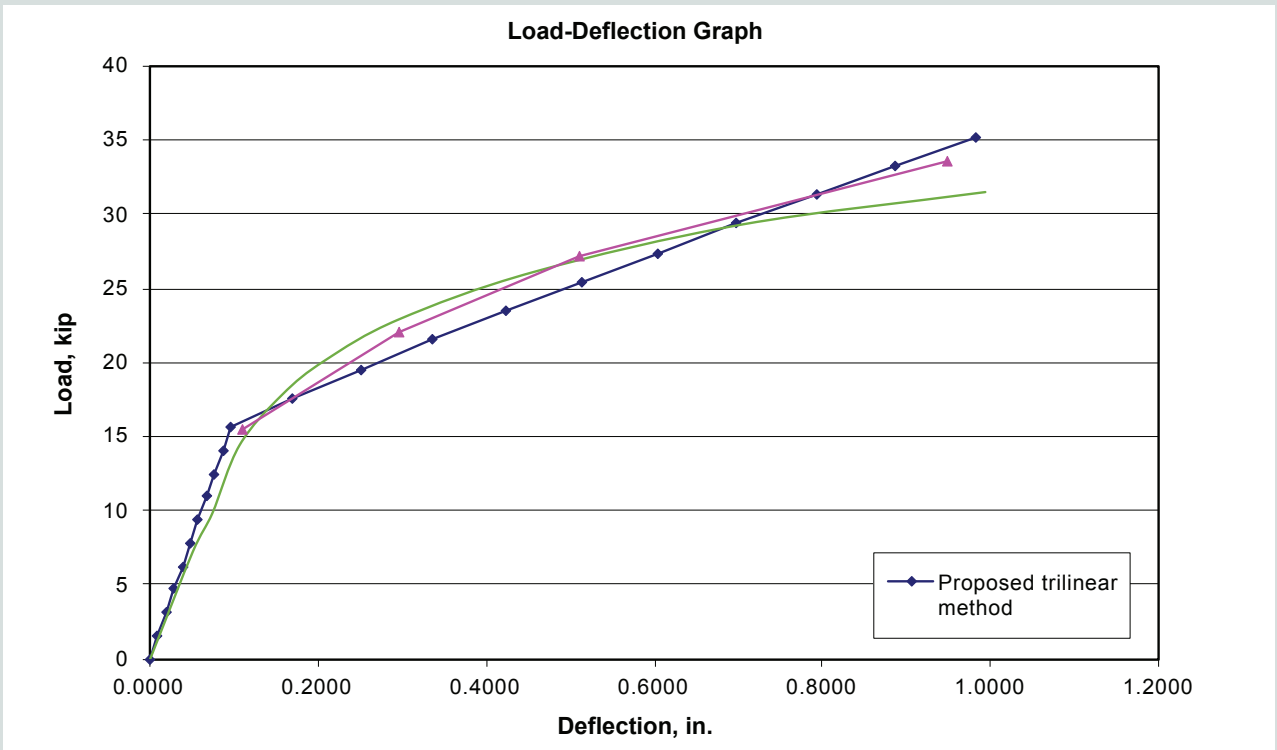

Figure 13. Load-deflection graph for beam 3 in Burns and Warwaruk.
Sources: Data from Burns (1964) and Warwaruk (1965).
Note: PCI 9-1 numerical method = numerical analysis results presented in Burns. 1 in. = 25.4 mm; 1 kip = 4.448 kN.

Table 2. Specimen data from Paranagama and Edwards

Beam mark	Height, in.	Width, in.	Prestressing depth, in.	f'_c, psi	f_{se}, ksi	A_{ps}, in.^{2}
A1	8	4	5.39	5065	35	0.09
B1	8	4	5.44	5430	46	0.09

Source: Data from Paranagama and Edwards (1969).

Note: A_{ps} = area of prestressing steel; f'_c = design compressive strength of concrete; f_{se} = initial tensioning stress in the prestressing steel after losses.1 in. = 25.4 mm; 1 in.2 = 654.2 mm2; 1 psi = 6.895 kPa; 1 ksi = 6.895 MPa.

moment-curvature data, not load deflection data for the test specimens; therefore, the loading setup is not as important as material properties and cross-section layout. The concrete used for the specimens had a ⅜ in. (9.5 mm) maximum aggregate size and a cylinder strength ranging from 3850 to 5550 psi (26.5 to 37.9 MPa). All beams had stirrups at 4.5 in. (114 mm) spacing.

The presence of the confinement steel allowed the concrete to reach higher compressive strains than ultimate useful compressive strain of 0.003 before failure; however, the proposed method does not take into account the effect of confinement steel. In **Fig. 14**, the beams exhibit greater curvatures and ultimate moments compared to predictions from the conservative proposed method that does not account for the confinement reinforcement (ultimate useful compressive strain of 0.003). Despite this conservatism, the proposed method remains applicable for the beams presented by Paranagama and Edwards.[12] The experimental data assumed zero curvature of the beam without an external load applied. Consequently, the proposed method was artificially zeroed for meaningful comparisons. In addition, a prestressing strand yield strain of 0.0087 was used in the proposed method for this comparison, instead of the typical strain of 0.01, to align with the yield strain, 0.0087, specified by Paranagama and Edwards[12] in their tests.

Beam A1 was the statically loaded control beam for the balanced design case. In Fig. 14, the moment-curvature graph depicts the experimental data alongside results from the proposed method. Good correlation is shown between the proposed method and the experimental data for the range of the proposed method. The predicted cracking, yielding, and ultimate points exhibit particularly strong alignment with the corresponding experimental data; however, the influence

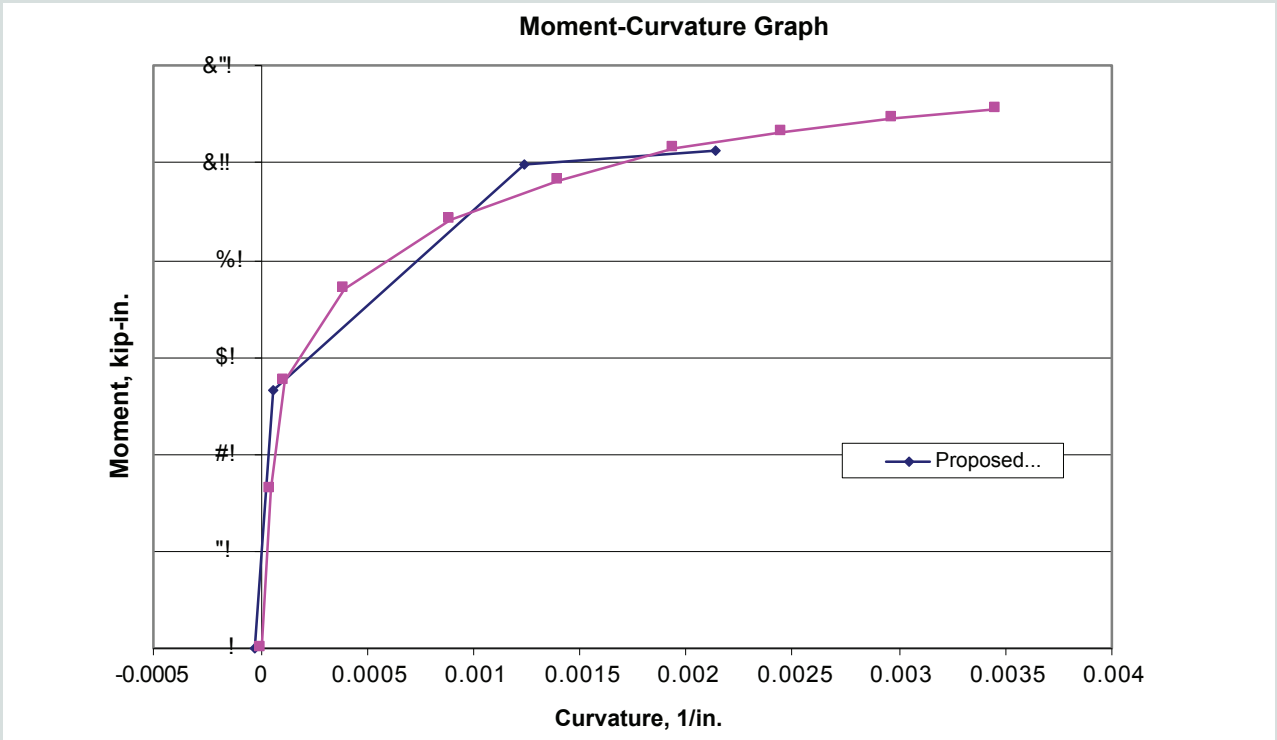

Figure 14. Moment-curvature graph for beam A1 in Paranagama and Edwards.
Source: Data from Paranagama and Edwards (1969).
Note: 1 in. = 25.4 mm; 1 kip-in. = 0.113 kN-m.

of confinement becomes evident through the larger ultimate moment and corresponding curvature of the experimental data.

Beam B1 was the statically loaded control beam for the underreinforced design case. **Figure 15** presents the moment-curvature responses for the experimental data and the proposed method. Figure 15 shows good correlation between the proposed method and the experimental data, except for the additional moment and curvature in the experimental data (the continuation of the solid pink line with squares) due to the confinement effect.

The moment-curvature graphs for beams A1 and B1 reveal only minor differences, suggesting that beam B1 was only slightly underreinforced; however, several differences between the two specimens exist. First, B1 exhibits a higher initial prestressing strain than A1. The higher initial strain leads to the higher cracking moment for B1, although it does not significantly affect the ultimate moment or curvature. Second, the final curvature for B1 is noticeably larger. Beams A1 and B1 have the same amount of prestressing steel, and so the difference in final curvature is caused by the effective depth of the prestressing strand. The effective depth for B1 is 5.44 in. (138 mm), compared with 5.39 in. (137 mm) for A1. The larger prestressing strand depth for B1 leads to a larger prestressing strain to achieve a concrete compression failure, which governs the ultimate condition of the beams. Therefore, the larger prestressing strain leads to a larger curvature. In addition, as the moment arm and prestressing force change, the ultimate moment changes slightly.

Beams tested by Rasheed et al.

Rasheed et al.[13] presented experimental data pertaining to four prestressed concrete tapered-web T girders strengthened with fiber-reinforced polymer, and one control beam (beam 1) that did not have any external fiber-reinforced polymer. Cross-section properties for all the beams are the same, except for the fiber-reinforced polymer. The gross cross section was a tapered T section with a flange width of 18 in. (450 mm) and a flange depth of 4 in. (100 mm). The web tapered from 6 in. (150 mm) at the flange-web junction to 4 in. at the bottom of the beam. The total height of the cross section was 14 in. (350 mm). Two straight strands of ⅜ in. (9.5 mm) diameter, 270 ksi (1860 MPa) low-relaxation prestressing steel were placed at 2 in. (50 mm) and 4 in. from the bottom of the cross section. The girder had mild compression steel and shear reinforcement. The initial stress in prestressing strand was 165 ksi (1140 MPa) after losses. A crack former was used to precrack the beams at the midspan.

The use of a tapered T section is outside the scope of the proposed analysis method; however, reasonable results were determined with five assumptions: an average web width was used; mild steel in the tension region of the cracked section was neglected for simplicity; the mild steel in the compression region was lumped at the centroid of the compression steel; the prestressing strand was located at its centroid; and

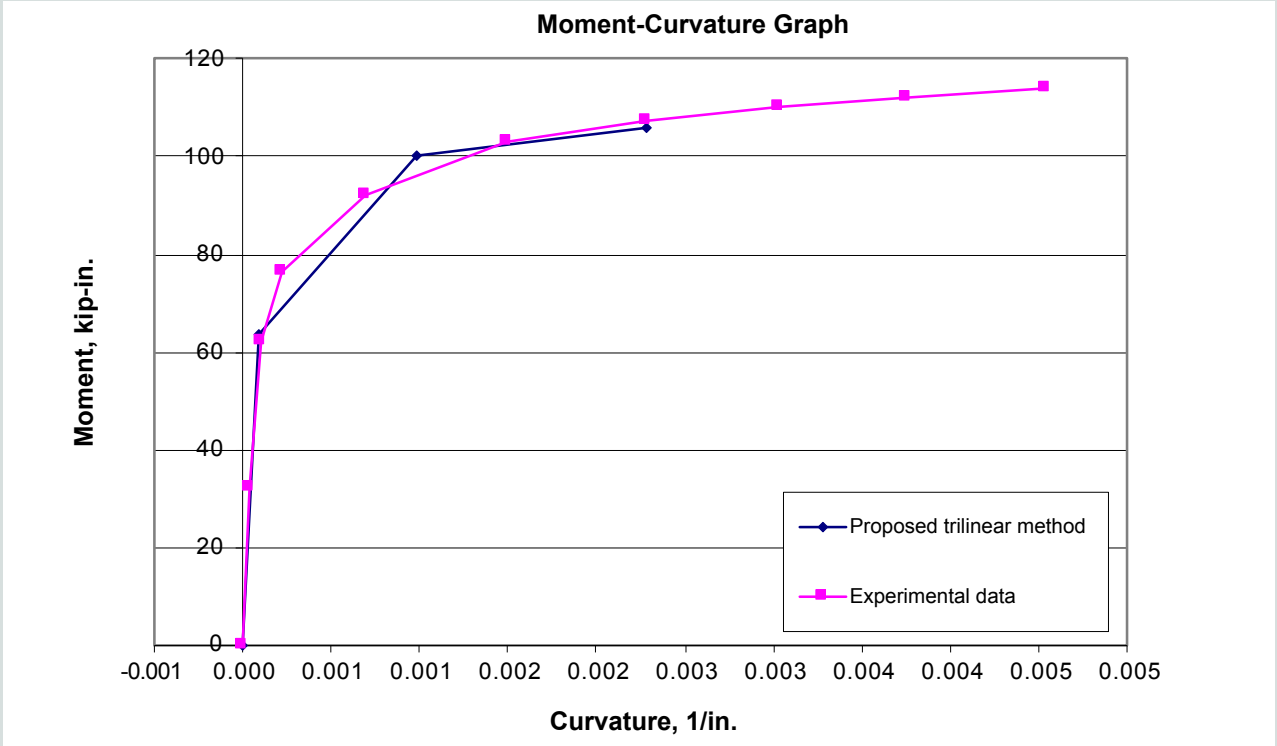

Figure 15. Moment-curvature graph for beam B1 in Paranagama and Edwards.
Source: Data from Paranagama and Edwards (1969).
Note: 1 in. = 25.4 mm; 1 kip-in. = 0.113 kN-m.

the precracking of the beam was ignored for initial point and cracking point calculations.

Figure 16 compares curves for the experimental (shown by solid orange lines with triangles), numerical (shown by solid blue line with diamonds for the uncracked and by solid pink line with squares for pre-cracked), and proposed trilinear method (shown by solid green lines with x's) load-deflection data pertaining to the control beam. The linear elastic region of the load-deflection response shows excellent (almost identical) correlation between the experimental data and the proposed method. The cracking point was adjusted because a crack former was used. Therefore, an experimentally measured bond stress ($4\sqrt{f'_c}$) between steel and concrete was used instead of the modulus of rupture of concrete to determine the cracking point. The yielding point and ultimate moment of the proposed method have relatively good correlation to the experimental data except a large discrepancy between the ultimate deflections occurred. The experimental test was performed in load control, which record large displacements at the failure load. The deflection of the proposed procedure still yields a larger deflection at failure than the other numerical responses. This difference may be because the incremental numerical analysis misses the exact failure load within the increments whereas the proposed procedure exactly determines the ultimate point.

The stress in the prestressing strand-applied moment curve can be determined from the proposed method. The initial stress in the prestressing strand is known from determining the initial prestressing force P_e. For the control beam, the initial stress in the prestressing strand was 165 ksi (1140 MPa) after losses. The stress in the prestressing strand at cracking is determined by adding the change in strain at the prestressing level from the initial point to the strain caused by the initial stress in the prestressing strand. Then the stress in the prestressing strand is determined from the stress-strain curve for 270 ksi (1860 MPa) low-relaxation prestressing strand. The yielding strain in the prestressing steel is known, so the stress is determined from the stress-strain curve. In addition, because the failure mode for the beam was strand rupture, the ultimate strain is also known, and the ultimate stress can be determined from the stress-strain curve. All of the applied moments are known from determining the trilinear moment-curvature response. **Figure 17** shows the numerical stress-moment curve presented by the Rasheed et al.13 and the stress-moment curve from the proposed trilinear method. Figure 17 shows good correlation between the two curves for the uncracked region; however, as the yielding and ultimate moments for the proposed method are less than the numerical analysis, the curves begin to deviate after the cracking point. Nevertheless, the proposed method provides a conservative estimation of the stress in the prestressing strand due to the applied moment. The determination of the stress-moment curve is required to determine the change in stress in the prestressing strand at service live loads. The American Association of State Highway and Transportation Officials' *AASHTO LRFD Bridge Design Specifications*[14] limit the change to 18 ksi (120 MPa) for straight strands.

Conclusion

The proposed trilinear method provides a reliable moment-curvature response and accurate closed-form short-

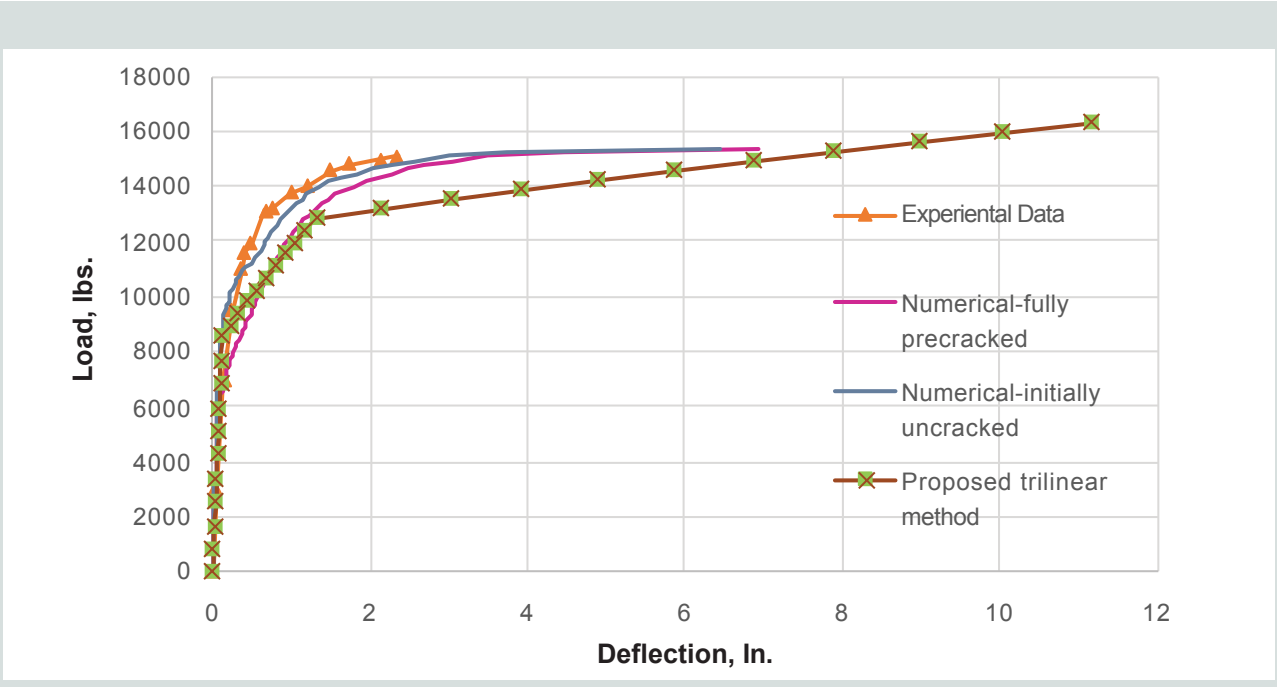

Figure 16. Load-deflection graph for control beam in Rasheed et al.
Source: Data from Rasheed et al. (2006).
Note: 1 in. = 25.4 mm; 1 lb = 4.448 N.

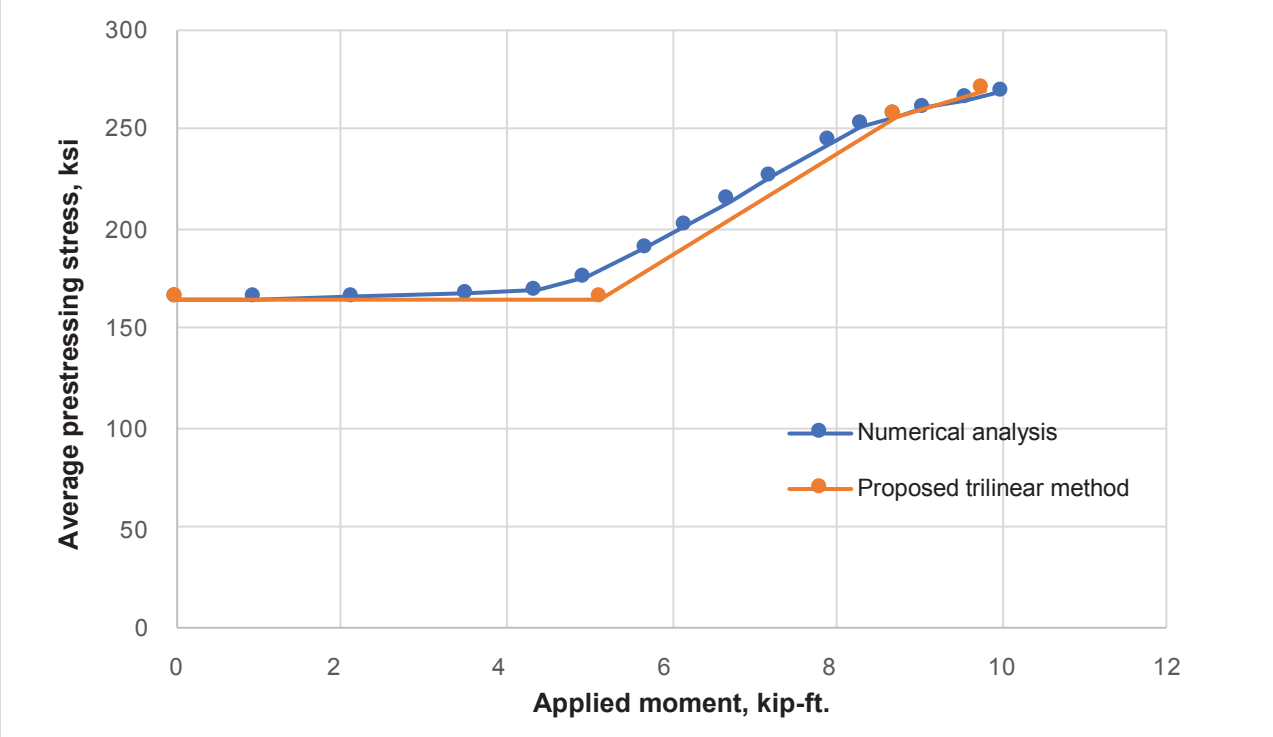

Figure 17. Prestress-applied moment graph for control beam in Rasheed et al.
Source: Data from Rasheed et al. (2006).
Note: 1 kip-ft = 1.356 kN-m; 1 ksi = 6.895 MPa.

term deflection predictions for prestressed concrete components with fully bonded, straight strands. The predictions are accurate for the entire component response, including the postyielding region. Overall, the proposed method correlates well with both the experimental and numerical results from the literature. This method may be used as a valuable tool for determining analytical nonlinear predictions. The effect of confinement steel was neglected and the compressive concrete failure strains were limited to 0.003 in the proposed method, which led to conservative predictions for some components that failed in concrete crushing. It is assumed that the trilinear moment-curvature response provides some tension stiffening in the postcracking region (before yielding) of the proposed method because the component is not completely cracked.

Because the proposed method accurately determines the failure mode, it improves the designer's understanding of a component's structural response failing in concrete crushing or strand rupture. The proposed method produces accurate predictions for the specific cross sections and loading patterns presented, and it is intended to be used following ACI 318-19 guidelines for prestressed concrete flexural components in analytical design computations.

References

1. Branson, D. E., and F. Shaikh. 1985. "Deflection of Partially Prestressed Members." *ACI Symposium*, no. 86, 323–364.
2. Alameh, A. S., and M. H. Harajli. 1989. "Deflection of Progressively Cracking Partially Prestressed Concrete Flexural Members." *PCI Journal* 34 (3): 94–128. https://doi.org/10.15554/pcij.05011989.94.128.
3. PCI (Precast/Prestressed Concrete Institute). 2017. *PCI Design Handbook: Precast and Prestressed Concrete*. 8th ed. Chicago, IL: PCI.
4. ACI (American Concrete Institute). 2019. *Building Code Requirements for Structural Concrete (ACI 318-19) and Commentary (ACI 318R-19).* Farmington Hills, MI: ACI.
5. Kramer, K. W., and H. A. Rasheed. 2018. "Analytical Load-Deflection Behavior of Prestressed Concrete Girders Strengthened with FRP." *ACI Symposium* 327: 13.1–13.20. https://doi.org/10.14359/51713334.
6. Hognestad, E. 1952. "Fundamental Concepts in Ultimate Load Design of Reinforced Concrete Members." *ACI Journal* 48 (6): 809–830. https://doi.org/10.14359/11956.
7. Park, R., and T. Paulay. 1975. *Reinforced Concrete Structures*. New York, NY: Wiley.
8. Charkas, H., H. A. Rasheed, and H. Melhem. 2003. "Rigorous Procedure for Calculating Deflections of Fiber-Reinforced Polymer-Strengthened Reinforced Concrete Beams." *ACI Structural Journal* 100 (4):

529–539. https://doi.org/10.14359/12662.

9. Warwaruk, J., M. A. Sozen, and C. P. Siess. 1962. *Strength and Behavior in Flexure of Prestressed Concrete Beams*. Champaign: University of Illinois Engineering Experiment Station.

10. Warwaruk, J. 1965. "Deformation Analysis for Prestressed Concrete Beams." *PCI Journal* 10 (5): 65–80. https://doi.org/10.15554/pcij.10011965.67.80.

11. Burns, N. H. 1964. "Moment Curvature Relationships For Partially Prestressed Concrete Beams." *PCI Journal* 9 (1): 52–63.

12. Paranagama, D. O., and A. D. Edwards. 1969. "Moment-Deformation Characteristics of Pretensioned Concrete Beams Subjected to Fluctuating Loads." *PCI Journal* 14 (4): 62–74. https://doi.org/10.15554/pcij.08011969.62.74.

13. Rasheed, H.A., Larson, K., and Peterman, R. 2006, "Analysis and Design Procedure for FRP-Strengthened Prestressed Concrete T-Girders Considering Strength and Fatigue." *Journal of Composites for Construction* 10(5): 419-432. https://doi.org/10.1061/(ASCE)1090-0268(2006)10:5(419).

14. AASHTO (American Association of State Highway and Transportation Officials). 2024. *AASHTO LRFD Bridge Design Specifications*, 10th ed. Washington, DC: AASHTO.

Notation

A_{gt} = gross area of the transformed section

A_{ps} = area of prestressing steel

= area of compression reinforcement

b = section width

b_f = flange width

b_w = web width

c_n = depth of the section neutral axis at ultimate strength

c_y = depth of the section neutral axis at first yielding

C = concrete compressive force

C_s = compressive force in the compression reinforcement

C_1 = first compressive force

C_2 = second compressive force

d = depth from the top of the section to the prestressing steel

d' = depth from the top of the section to the compression reinforcement

e = eccentricity of prestressing strands to the center of gravity of the transformed section

E = modulus of elasticity

E_c = modulus of elasticity of concrete

E_{ps} = modulus of elasticity of the prestressing strands

E_s = modulus of elasticity of the mild reinforcement

f_{bot} = stress in the extreme bottom fibers

f_c = concrete compressive stress

= design compressive strength of concrete

f_{ps} = stress in the prestressing steel

f_{pu} = ultimate stress of the prestressing steel

f_{py} = yield stress of the prestressing steel

f_r = concrete rupture strength

= stress in the compression reinforcement

f_{se} = initial tensioning stress in the prestressing steel after losses

f_{top} = stress in the extreme top fiber

f_y = yield stress of the mild reinforcement

h = height of the section

I = moment of inertia

I_g = gross moment of inertia

I_{gt} = gross moment of inertia of the transformed section

I_n = moment of inertia at the nominal moment

I_y = moment of inertia at yield

L = span length

L_a = length from the support to the load application point

L_g = length from the support to the cracking moment location (uncracked region)

L_y = length from the support to the yield moment location

M = moment

$M(x)$ = moment expression as a function of x

M_a = moment at the load application point

M_{cr} = cracking moment

M_n = nominal ultimate moment

M_u = ultimate moment

M_y = moment at yield

P = point load

P_e = prestressing force

r_2 = the square of the radius of gyration

t_f = flange thickness

T = tensile force

w = uniform load

x = location along the beam measured from the support

x_1 = constant based on the yield strength of the prestressing strand

y_{bot} = distance from the bottom of the section to the neutral axis

y_t = distance between the neutral axis of the uncracked transformed section to the extreme fiber in tension

y_{top} = distance from the top of the section to the neutral axis

α = factor for the height of the equivalent rectangular stress block

α_1 = proportional factor for the height of the equivalent rectangular stress block corresponding to C_1

α_2 = proportional factor for the height of the equivalent rectangular stress block corresponding to C_2

γ = neutral axis multiplier

γ_1 = neutral axis multiplier corresponding to C_1

γ_2 = neutral axis multiplier corresponding to C_2

γ_y = neutral axis multiplier corresponding to c_y

δ_1 = deflection for the uncracked region

δ_2 = deflection for the postcracked region

δ_3 = deflection for the postyielding region

$\Delta_{midspan}$ = midspan deflection

ε_{bot} = strain at the bottom of the section

ε_c = concrete strain

= strain at maximum compressive stress

ε_{cf} = extreme compressive fiber strain

ε_{cu} = extreme compressive fiber strain at concrete crushing

ε_{cw} = the strain at the compressive flange-web junction

ε_{ps} = strain in the prestressing strand

ε_{psy} = yield strain of the prestressing steel

= strain in the compression reinforcing steel

ε_{top} = strain at the top of the section

ε_1 = strain due to the initial tensioning stress in the prestressing steel after losses

ε_2 = strain due to the decompression of the section at the level of the prestressing strands

ε_3 = remaining strain in the prestressing strand required for strain compatibility

ϕ_a = curvature corresponding to maximum moment

ϕ_{cr} = curvature at the cracking moment location

ϕ_{in} = initial curvature

ϕ_n = curvature at the nominal ultimate moment location

ϕ_{pc} = curvature for postcracked region

ϕ_{py} = curvature for postyielding region

ϕ_{un} = curvature for uncracked region

ϕ_y = yield point curvature

$f(x)$ = generic curvature expression for a beam

About the authors

Kimberly Waggle Kramer, PhD, PE, SE, is a professor in the G. E. Johnson Department of Architectural Engineering and Construction Science at Kansas State University in Manhattan.

Hayder A. Rasheed, PhD, PE, is a professor in the Department of Civil Engineering at Kansas State University in Manhattan.

Steven R. Peterson, EIT, is a structural engineering staff for 10Fold Architecture and Engineering, Ames, Iowa.

Abstract

In this paper, a trilinear moment-curvature response is assumed to govern the behavior of prestressed concrete beams with straight strands. The trilinear moment-curvature response is integrated to yield closed-form deflection expressions that are useful for analytically assessing the deflections of prestressed concrete flexural members. To evaluate the key controlling points of the moment-curvature relationship, the derived procedure used closed-form and iterative equations to determine neutral axis locations, moments, and curvatures at the cracking, yielding, and ultimate levels to define the trilinear moment-curvature response. To derive the equations, internal stress analysis was used for the linear-elastic region upon cracking and strain compatibility and force equilibrium were used for the postcracked regions of the response, along with nonlinear material behaviors. Both strand ultimate strain and concrete crushing failure modes were analyzed for each cross section. Previously published experimental data for six prestressed concrete beams were used to check the derived short-term deflection analysis procedure. Of the six specimens, some had moment-curvature graphs and others had load-deflection graphs that could be used for comparison to the equations in the proposed method. The proposed method produced accurate predictions for moment-curvature and short-term load-deflection responses, and it determined deflections within the postyielding region of the load-deflection response that are not accurately predicted by methods in the American Concrete Institute's *Building Code Requirements for Structural Concrete (ACI 318-19) and Commentary (ACI 318R-19)* or the eighth edition of the *PCI Design Handbook*.

Keywords

Closed-form deflection; cracked section; girder; moment curvature; prestressed concrete girder.

Review policy

This paper was reviewed in accordance with the Precast/Prestressed Concrete Institute's peer-review process. The Precast/Prestressed Concrete Institute is not responsible for statements made by authors of papers in *PCI Journal*. No payment is offered.

Publishing details

This paper appears in *PCI Journal* (ISSN 0887-9672) V. 71, No. 1, January–February 2025, and can be found at https://doi.org/pcij71.1-03. *PCI Journal* is published bimonthly by the Precast/Prestressed Concrete Institute, 8770 W. Bryn Mawr Ave., Suite 1150, Chicago, IL 60631.

Reader comments

Please address any reader comments to *PCI Journal* editor-in-chief Tom Klemens at tklemens@pci.org or Precast/Prestressed Concrete Institute, c/o *PCI Journal*, 8770 W. Bryn Mawr Ave., Suite 1150, Chicago, IL 60631.